J Math Imaging Vis (2014) 49:611–632
DOI 10.1007/s10851-013-0491-y

Suboptimal Solutions to the Algebraic-Error Line Triangulation

Qiang Zhang · Yan Wu · Fan Wang · Qiulei Dong · Licheng Jiao

Received: 21 November 2012 / Accepted: 31 December 2013 / Published online: 14 January 2014

Abstract Line triangulation, a foundational problem in computer vision, is to estimate the 3D line position from a set of measured image lines with known camera projection matrices. Aiming to improve the triangulation's efficiency, in this work, two algorithms are proposed to find suboptimal solutions under the algebraic-error optimality criterion of the Plücker line coordinates. In these proposed algorithms, the algebraic-error optimality criterion is reformulated by the transformation of the Klein constraint. By relaxing the quadratic unit norm constraint to six linear constraints, six new single-quadric-constraint optimality criteria are constructed in the new formulation, whose optimal solutions can be obtained by solving polynomial equations. Moreover, we prove that the minimum algebraic error of either the first three or the last three of the six new criteria is not more than $\sqrt{3}$ times of that of the original algebraic-error optimality criterion. Thus, with three new criteria and all the six criteria, suboptimal solutions under the algebraic error minimization and the geometric error minimization are obtained. Experimental results show the effectiveness of our proposed algorithms.

Q. Zhang (✉) · Y. Wu · F. Wang
School of Electronic Engineering, Xidian University, Xi'an 710071, China
e-mail: zhangqiang@xidian.edu.cn

Q. Zhang · L. Jiao
Key Laboratory of Intelligent Perception and Image Understanding of Ministry of Education, Xidian University, Xi'an 710071, China

Q. Dong
National Laboratory of Pattern Recognition, Institute of Automation, Chinese Academy of Sciences, Beijing 100190, China

Keywords Line triangulation · Multiple views · Algebraic error · Plücker line coordinates · Suboptimal solutions

1 Introduction

In computer vision, triangulation is to determine the 3D position of a feature given its projections onto multiple images and the corresponding camera projection matrices. In literature, the triangulation of 3D points [1–10] has been investigated extensively. As the reconstruction of manmade scenes has become a hot topic [11–13] in recent years, lines, which are widely available in manmade scenes and provide more information about scene geometrical structure, need special consideration. Compared with point feature, lines have their own specialties in triangulation [14]. For example, projected image lines can be extracted more accurately and are less sensitive to occlusion. And because 3D line has 4 degrees of freedom to represent, there does not exist any simple representation for it [15]. In addition, line triangulation, especially those involving more than three cameras, is more difficult to handle in itself than point triangulation.

In recent years, line triangulation has drawn more and more attention and some algorithms have been proposed based on different line representations. Early works mainly focused on triangulation for only three cameras [16, 17], while recent works addressed the multiple-view line triangulation problem for improving the triangulation's accuracy. Based on the Plücker line coordinates and the algebraic-error cost function, three algorithms were proposed to solve the multiple-view triangulation problem in [15]. Because the optimality criteria of these algorithms do not enforce the Klein constraint, their solutions are sensitive to measurement errors. Also based on the Plücker line coordinates, an algorithm [18] is proposed to minimize the geometric

error under the L_2-norm, where the solution could satisfy the Klein constraint, but the introduced algorithm is of high computational complexity. In addition, in the Gold Standard algorithm [19], because a complex geometric-error cost function, which is constructed via projections on two images and the trifocal tensors, is solved by the Levenberg-Marquardt method, the involved computational load is large and the solution seems sensitive to the choice of the two projections.

To well balance the reconstruction accuracy and the computational efficiency of multiple-view line triangulation, two suboptimal algorithms are proposed for the algebraic-error minimization based line triangulation. In this work, the algebraic-error optimality criterion is reformulated by the transformation of the Klein constraint. And under the new formulation, by relaxing the original quadratic unit norm constraint on the Plücker line coordinates to six simple linear ones, six new single-quadric-constraint optimality criteria are constructed, where the corresponding optimal solutions satisfy the Klein constraint and can be obtained by solving polynomial equations. In addition, we give a formal proof that the minimum algebraic error of either the first three or the last three of the six new criteria is not more than $\sqrt{3}$ times of that of the original algebraic-error optimality criterion. Therefore, via either three new criteria or all the six new criteria, two suboptimal solutions to the algebraic error minimization or the geometric error minimization can be obtained. Compared with the linear algorithm, the quasi-linear algorithms [15], and the Gold Standard algorithm [19], our two new suboptimal algorithms are shown to be both accurate and efficient with extensive experimental results.

The remainder of this paper is organized as follows: Sect. 2 is a short review of the Plücker line coordinates and the line projection matrix. In Sect. 3, the algebraic-error optimality criterion is introduced. Section 4 elaborates our unit norm relaxation technique, new single-quadric-constraint optimality criteria construction and the definition of the two suboptimal solutions. In Sect. 5, the process of solving the new optimality criteria is presented. Section 6 reports the experimental results. Section 7 concludes this paper.

2 Plücker Line Coordinates and Associated Line Projection Matrix

A 3D line has 4 degrees of freedom, it cannot be simply represented in P^3. Among the possible representations in the literature, Plücker line coordinates [15, 20] is the most popular one.

Given two 3D points $\mathbf{X} \sim (\mathbf{x}^T, m)^T$, $\mathbf{Y} \sim (\mathbf{y}^T, n)^T$ in P^3, the Plücker coordinates of the line joining them is a 6-vector $\mathbf{L} \sim (\mathbf{a}^T, \mathbf{b}^T)^T$:

$$\begin{aligned} \mathbf{a} &= m\mathbf{y} - n\mathbf{x} \\ \mathbf{b} &= \mathbf{x} \times \mathbf{y} \end{aligned} \tag{1}$$

Note that not all the vectors in the 6-dimensional space are the Plücker line coordinates. For $\mathbf{L} \sim (\mathbf{a}^T, \mathbf{b}^T)^T$ to be a true line representation, it must satisfy the following bilinear constraint, called Klein constraint:

$$\mathbf{a}^T\mathbf{b} = 0 \tag{2}$$

Under the Plücker line coordinates, the line projection matrix, which describes the central projection mapping from 3D lines to image lines, is defined as:

Definition 1 Given $\mathrm{P} = (\mathbf{p}_1, \mathbf{p}_2, \mathbf{p}_3, \mathbf{p}_4)$ as the point projection matrix, where $\mathbf{p}_i$ is the ith column in P. Then, the line projection matrix Q is given by

$$\mathrm{Q} = (\mathbf{p}_4 \times \mathbf{p}_1, \mathbf{p}_4 \times \mathbf{p}_2, \mathbf{p}_4 \times \mathbf{p}_3, \mathbf{p}_2 \times \mathbf{p}_3, \mathbf{p}_3 \times \mathbf{p}_1, \mathbf{p}_1 \times \mathbf{p}_2).$$

Therefore, the projection relation between 3D line and image line can be written as

$$\mathbf{l} \sim \mathrm{Q}\mathbf{L} \tag{3}$$

3 Algebraic-Error Optimality Criterion

Based on the above-defined line projection matrix, we can obtain the following two constraints between a 3D line $\mathbf{L}$ and the two endpoints $\{\mathbf{x}_{i1}, \mathbf{x}_{i2}\}$ of its projected image line in the ith image

$$\begin{cases} \mathbf{x}_{i1}^T\mathrm{Q}_i\mathbf{L} = 0, \\ \mathbf{x}_{i2}^T\mathrm{Q}_i\mathbf{L} = 0, \end{cases} \quad i = 1, 2, \ldots, n \tag{4}$$

where Q_i is the line projection matrix of the ith camera. Since various noises are inevitable, the constraints in (4) cannot be strictly satisfied in practice, hence we have:

$$\begin{cases} \mathbf{x}_{i1}^T\mathrm{Q}_i\mathbf{L} = \varepsilon_{i1}, \\ \mathbf{x}_{i2}^T\mathrm{Q}_i\mathbf{L} = \varepsilon_{i2}, \end{cases} \quad i = 1, 2, \ldots, n \tag{5}$$

where $\varepsilon_{i1}, \varepsilon_{i2}$ $(i = 1, 2, \ldots, n)$ are the algebraic errors of the ith camera. In this paper, the algebraic error, i.e. the L_2-norm of algebraic errors in all the cameras, will be minimized, called under the algebraic-error optimality criterion, to estimate 3D line coordinates $\bar{\mathbf{L}}$ as:

$$\begin{array}{lll} \min & \displaystyle\sum_{i=1}^{n} \varepsilon_{i1}^2 + \varepsilon_{i2}^2 & \min \quad \bar{\mathbf{L}}^T\mathrm{A}^T\mathrm{A}\bar{\mathbf{L}} \\ \text{s.t.} & \bar{\mathbf{L}}^T\mathrm{G}\bar{\mathbf{L}} = 0 \quad \Leftrightarrow & \text{s.t.} \quad \bar{\mathbf{L}}^T\mathrm{G}\bar{\mathbf{L}} = 0 \\ & \bar{\mathbf{L}}^T\bar{\mathbf{L}} = 1 & \quad\quad \bar{\mathbf{L}}^T\bar{\mathbf{L}} = 1 \end{array} \tag{6}$$

where $\mathrm{A} = (\ldots, \mathrm{Q}_i^T \mathbf{x}_{i1}, \mathrm{Q}_i^T \mathbf{x}_{i2}, \ldots)^T$, $i = 1, 2, \ldots, n$, $\mathrm{G} = \begin{pmatrix} 0 & \mathrm{I}_3 \\ \mathrm{I}_3 & 0 \end{pmatrix}$, I_3 is the 3×3 identity matrix, and $\bar{\mathbf{L}}^T \mathrm{G} \bar{\mathbf{L}} = 0$ is equivalent to the Klein constraint (2). $\bar{\mathbf{L}}^T \bar{\mathbf{L}} = 1$ is the unit norm constraint to avoid the trivial solution $\bar{\mathbf{L}} = 0$ and limit the solution space to a compact set. Because the algebraic-error optimality criterion (6) has two quadric constraints on $\bar{\mathbf{L}}$, it is very difficult to obtain the global optimal solution. A linear algorithm is proposed in [15] to divide the process of solving the minimization problem (6) into two steps:

(1) Solve the least-squares problem as follows

$$\begin{aligned} \min \quad & \bar{\mathbf{L}}^T \mathrm{A}^T \mathrm{A} \bar{\mathbf{L}} \\ \text{s.t.} \quad & \bar{\mathbf{L}}^T \bar{\mathbf{L}} = 1 \end{aligned}$$

(2) Use the Plücker correction to find a Plücker-coordinates solution, which is the closest Plücker coordinates to the solution of step 1 under the L_2-norm.

Note that the linear algorithm in [15] is shown quite sensitive to noise from our experimental results in Sect. 6.

4 New Optimality Criteria and Suboptimal Solutions

In this section, six linear constraints are introduced to replace the unit norm constraint in (6), then the resulting minimization problems all contain only a single quadric constraint on the estimated Plücker line coordinates. By relaxing the unit norm constraint after reformulation of the original criterion (6), 6 new single-quadric-constraint minimizations are considered, hereinafter called 6 new optimality criteria. Finally based on the solutions of these 6 new optimality criteria, two suboptimal solutions of minimizing either the algebraic error or the geometric error are provided. In the next, such issues will be discussed in details.

To avoid the Plücker correction in [15] and ensure that the obtained solution is a Plücker line coordinates, the Klein constraint needs to be retained. In this work, the following six linear constraints are used to replace the unit norm constraint in (6)

$$\bar{\mathbf{L}}^T \mathbf{e}_j = 1, \quad j = 1, \ldots, 6 \tag{7}$$

where $\mathbf{e}_j$ is the unit vector whose jth element is one. Under these constraints, the jth coordinate of $\bar{\mathbf{L}}$ is one and the rest are still variants, which keeps the vector $\bar{\mathbf{L}}$ from becoming zero-vector. By replacing the unit norm constraint in (6) with the 6 linear constraints in (7), we obtain 6 single-quadric-constraint optimality criteria whose normalized solutions will still lie in the solution space of (6) and have a bounded minimum algebraic error compared with the minimum algebraic error of the original optimality criterion (6).

In order to further reduce the minimum-algebraic-error upper bound and the computational complexity, we at first reformulate the optimality criterion (6), and then construct our new single-quadric-constraint optimality criteria in what follows.

Let

$$\mathrm{V}_G \begin{pmatrix} \mathrm{I}_3 & 0 \\ 0 & -\mathrm{I}_3 \end{pmatrix} \mathrm{V}_G^T$$

be an eigen-decomposition of G, the Klein constraint can be transformed into

$$\tilde{\mathbf{L}} \begin{pmatrix} \mathrm{I}_3 & 0 \\ 0 & -\mathrm{I}_3 \end{pmatrix} \tilde{\mathbf{L}} = 0,$$

where

$$\tilde{\mathbf{L}} = \mathrm{V}_G^T \bar{\mathbf{L}}, \quad \mathrm{V}_G = \frac{1}{\sqrt{2}} \begin{pmatrix} \mathrm{J} & \mathrm{J} \\ \mathrm{J} & -\mathrm{J} \end{pmatrix} \quad \text{and}$$

$$\mathrm{J} = \begin{pmatrix} 0 & 1 & 0 \\ 1 & 0 & 0 \\ 0 & 0 & 1 \end{pmatrix}.$$

Obviously, the minimization problem (6) is equivalent to the following minimization problem

$$\begin{aligned} \min \quad & \tilde{\mathbf{L}}^T \mathrm{V}_G^T \mathrm{A}^T \mathrm{A} \mathrm{V}_G \tilde{\mathbf{L}} \\ \text{s.t.} \quad & \tilde{\mathbf{L}}^T \begin{pmatrix} \mathrm{I}_3 & 0 \\ 0 & -\mathrm{I}_3 \end{pmatrix} \tilde{\mathbf{L}} = 0 \\ & \tilde{\mathbf{L}}^T \tilde{\mathbf{L}} = 1 \end{aligned} \tag{8}$$

To further reduce the complexity of the cost function, let the eigen-decomposition of the upper left 3×3 submatrix of $\mathrm{V}_G^T \mathrm{A}^T \mathrm{A} \mathrm{V}_G$ be $\mathrm{V}_1 \Sigma_1 \mathrm{V}_1^T$, and the eigen-decomposition of the lower right 3×3 submatrix of $\mathrm{V}_G^T \mathrm{A}^T \mathrm{A} \mathrm{V}_G$ be $\mathrm{V}_2 \Sigma_2 \mathrm{V}_2^T$, then the criterion (8) can be simplified as:

$$\begin{aligned} \min \quad & \hat{\mathbf{L}}^T \begin{pmatrix} \Sigma_1 & \mathrm{B} \\ \mathrm{B}^T & \Sigma_2 \end{pmatrix} \hat{\mathbf{L}} \\ \text{s.t.} \quad & \hat{\mathbf{L}}^T \begin{pmatrix} \mathrm{I}_3 & 0 \\ 0 & -\mathrm{I}_3 \end{pmatrix} \hat{\mathbf{L}} = 0 \\ & \hat{\mathbf{L}}^T \hat{\mathbf{L}} = 1 \end{aligned} \tag{9}$$

where $\hat{\mathbf{L}} = \begin{pmatrix} \mathrm{V}_1^T & 0 \\ 0 & \mathrm{V}_2^T \end{pmatrix} \tilde{\mathbf{L}}$, $\mathrm{B} = (\mathrm{V}_1^T \ 0) \mathrm{V}_G^T \mathrm{A}^T \mathrm{A} \mathrm{V}_G \begin{pmatrix} 0 \\ \mathrm{V}_2 \end{pmatrix}$. In the criterion (9), the constraints are meant that the sum of squares of the first three coordinates of $\tilde{\mathbf{L}}$ is equal to 1/2, and so is the sum of squares of its last three coordinates. Thus, the transformed solution space in (9) is divided into two subspaces, i.e., the first three coordinates and the last three coordinates. Through the following inverse transformation, the solution of (9) can be transformed back to the solution space of (6), called the original-space solution of (9) here, by

$$\bar{\mathbf{L}} = \mathrm{V}_G \begin{pmatrix} \mathrm{V}_1 & 0 \\ 0 & \mathrm{V}_2 \end{pmatrix} \hat{\mathbf{L}} \tag{10}$$

Similarity by replacing the unit norm constraint in (9) by $\hat{\mathbf{L}}^T \mathbf{e}_j = 1$, $j = 1, \ldots, 6$, the following 6 new single-quadric-constraint optimality criteria are obtained, and the normal-

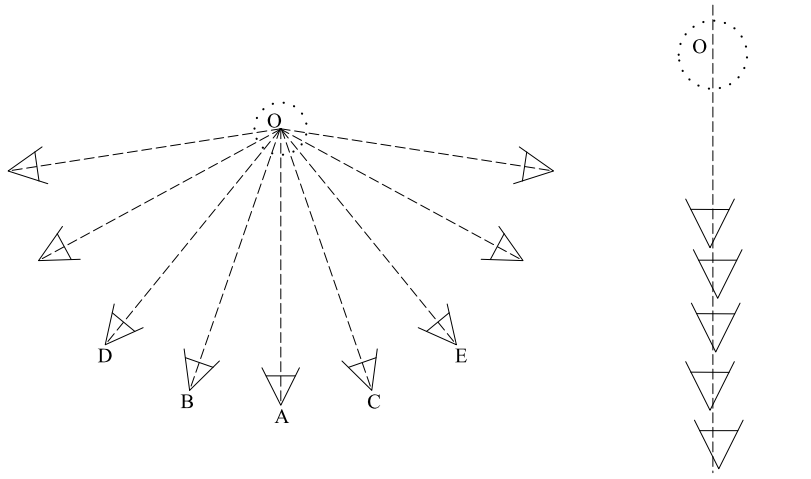

Configuration I Configuration II

Fig. 1 Two typical configurations used in the experiments. (*Left*) Circular configuration. (*Right*) Radial configuration

ized solutions of these new optimality criteria can satisfy the constraints in (9):

$$\begin{aligned} \min \quad & \hat{\mathbf{L}}^T \begin{pmatrix} \Sigma_1 & \mathrm{B} \\ \mathrm{B}^T & \Sigma_2 \end{pmatrix} \hat{\mathbf{L}} \\ \text{s.t.} \quad & \hat{\mathbf{L}}^T \begin{pmatrix} \mathrm{I}_3 & 0 \\ 0 & -\mathrm{I}_3 \end{pmatrix} \hat{\mathbf{L}} = 0, \quad j = 1, \ldots, 6 \\ & \hat{\mathbf{L}}^T \mathbf{e}_j = 1 \end{aligned} \tag{11}$$

Note that in these optimality criteria, since the unit norm constraint is relaxed, the resulting solution space is no longer a compact set. But with enough measured endpoints, the cost function is of a positive definite quadratic form which ensures the existence of its minimum. In addition, note that because of the transformed solution space, the new optimality criteria in (11) have a different upper bound of the minimum algebraic error and different conditions to obtain the upper bound, which will be stated in the following proposition.

Proposition 1 *The minimum algebraic error under the* 3 *normalized solutions of either the first three optimality criteria* ($j = 1, 2, 3$) *or the last three optimality criteria* ($j = 4, 5, 6$) *in* (11) *is not more than* $\sqrt{3}$ *times of the minimum algebraic error of the original optimality criterion* (6).

Proof In the transformed solution space of (9), because its two subspaces, i.e., the first three coordinates and the last three coordinates, are independent and have similar constraints, the same upper bounds of the minimum algebraic error can be obtained by just calculating their corresponding three criteria in (11). Thus, here we only discuss the case when the first three criteria ($j = 1, 2, 3$) are selected.

Suppose for $j = 1, 2, 3$, the optimal solutions of the three criteria in (11) are $\hat{\mathbf{L}}_j^{opt}$ and their corresponding minimum errors are err_{opt}^j. To satisfy the constraints of the criterion (9), $\hat{\mathbf{L}}_j^{opt}$ need to be normalized. Suppose the jth element of the normalized $\hat{\mathbf{L}}_j^{opt}$ is β_j, its algebraic error should be $err_{sopt}^j = |\beta_j| err_{opt}^j$. From the constraints of (9), it is known that $|\beta_j| \in (0, 1/\sqrt{2}]$. Similarly, suppose the optimal solution $\hat{\mathbf{L}}^{opt}$ of the criterion (9) has the algebraic error err_{opt} and its jth element is α_j. Since $\hat{\mathbf{L}}^{opt}/\alpha_j$ is not necessarily the optimal solution of (11), $err_{opt}^j \le err_{opt}/|\alpha_j|$, we have

$$err_{opt} \le err_{sopt}^j \le \left|\frac{\beta_j}{\alpha_j}\right| err_{opt}.$$

Here, we use err_{sopt} to represent the smallest value among err_{sopt}^j ($j = 1, 2, 3$), then the following inequalities hold

$$\begin{aligned} err_{opt} \le err_{sopt} &= \min_{j=1,2,3} err_{sopt}^j \\ &\le \min_{j=1,2,3} \left|\frac{\beta_j}{\alpha_j}\right| err_{opt} \\ &\le \frac{1/\sqrt{2}}{\max_{j=1,2,3} |\alpha_j|} err_{opt} \end{aligned} \tag{12}$$

As seen from the constraints of criterion (9), the maximum of $|\alpha_j|$ will be not less than $1/\sqrt{6}$, then $err_{sopt} \in [err_{opt}, \sqrt{3} err_{opt}]$. Because the minimum algebraic error of the criterion (6) are equal to that of the criterion (9), the algebraic error err_{sopt} is not more than $\sqrt{3}$ times of the minimum algebraic error of the original criterion (6). □

For the simplified criteria corresponding to the criterion (6), it also can be proven that the upper bound of the minimum algebraic error under all their six normalized solutions is not less than $\sqrt{5}$ times of the minimum algebraic

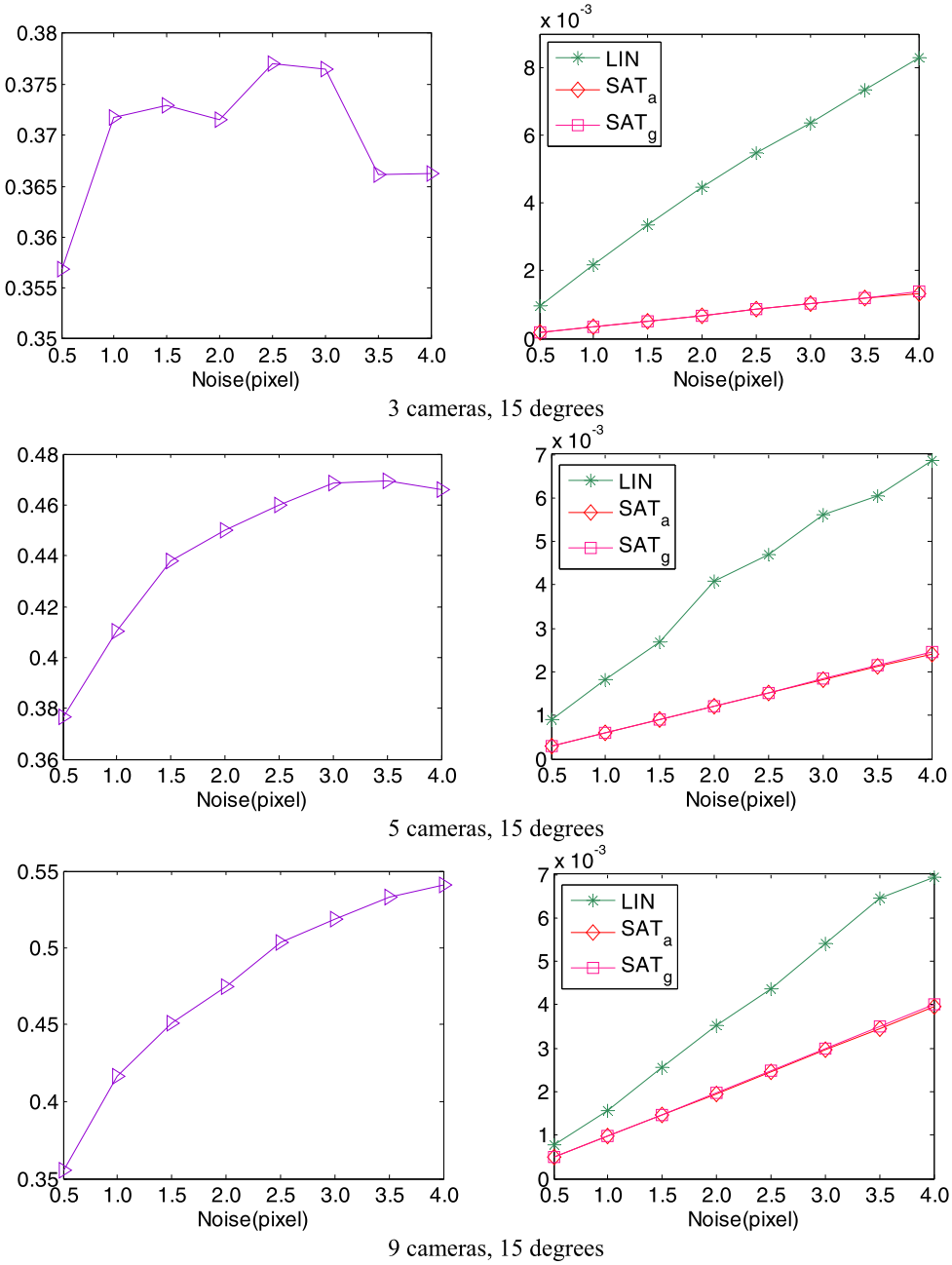

Fig. 2 Experimental results of the Configuration I. (*Left*) Result repeat ratio of the SAT_a and the SAT_g. (*Right*) RMS of algebraic error of the LIN, the SAT_a and the SAT_g

error of (6). By contrast, via the simple reformulation of the criterion (6), a lower upper bound of the minimum algebraic error can be obtained by solving only three of the six new criteria in (11). Thus, in this paper, the original-space solution, which corresponds to the smallest-algebraic-error solution of the three criteria in Proposition 1, is defined as the algebraic suboptimal solution of the optimality criterion (6). It should be noticed that the solution with a low algebraic error does not always mean a better 3D reconstruction. Thus, we select the solution from the original-space solutions of all the optimality criteria in (11) as the geometric suboptimal solution, which gives the smallest geometric error (i.e., the sum of squared distances from the measured image endpoints to the estimated image lines). Experiments in Sect. 6 show that the geometric suboptimal solution is more accurate and stable than the algebraic suboptimal solution.

5 Solutions to the New Optimality Criteria

In this section, we only provide the process of solving one of the 6 criteria in (11), say $j = 1$, the other 5 can be done sim-

Fig. 2 (*Continued*)

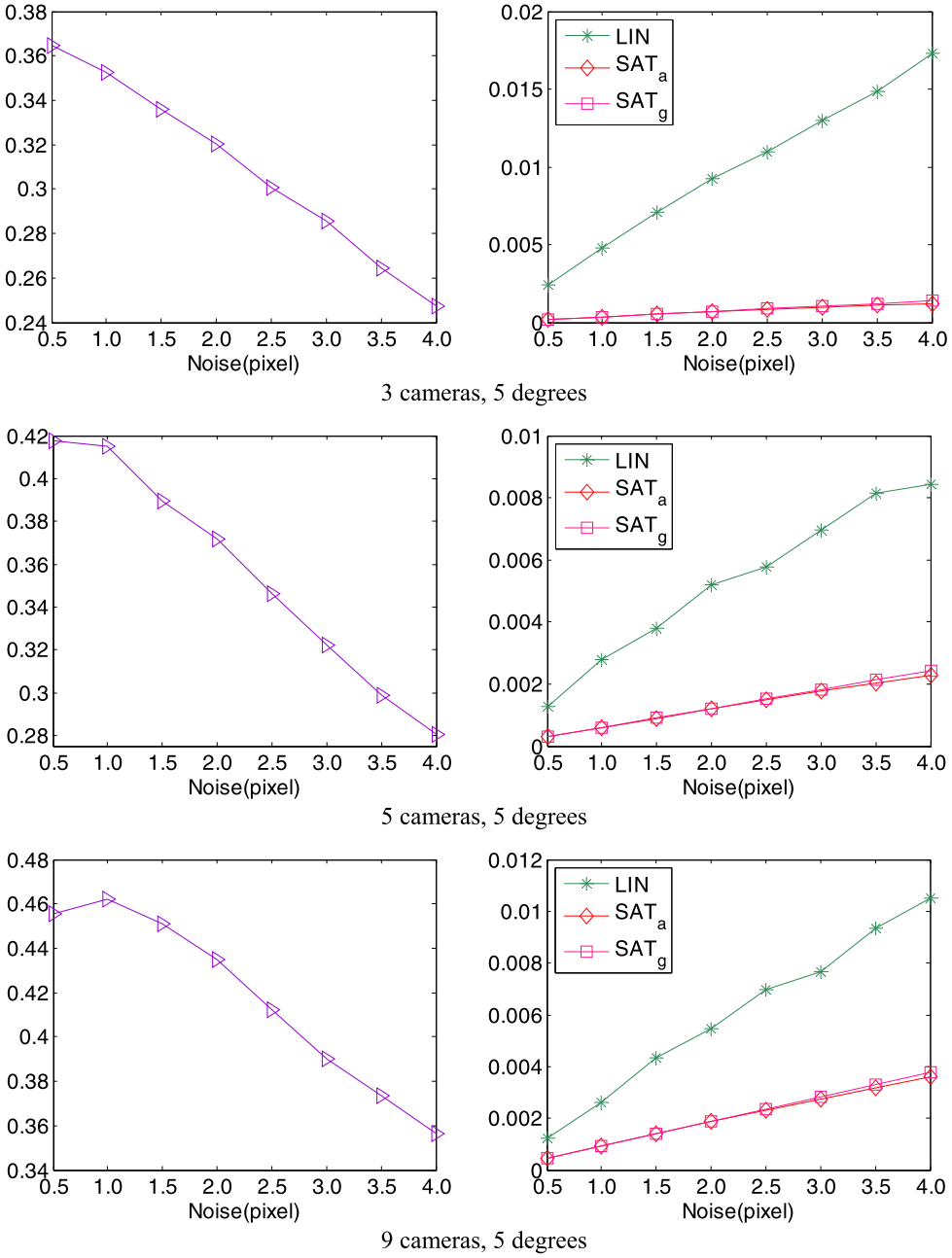

ilarly and will not be discussed. For notational convenience, $\hat{\mathbf{L}}_1$ is used to replace the constraint $\hat{\mathbf{L}}^T\mathbf{e}_1 = 1$, which means its first coordinate is fixed to 1 and the other five coordinates are variants.

The minimization problem for $\hat{\mathbf{L}}_1$ is

$$\begin{aligned} \min \quad & \sigma_1 + \hat{\mathbf{L}}_{1,2}^T \Sigma_1' \hat{\mathbf{L}}_{1,2} + 2\mathbf{B}_1 \hat{\mathbf{L}}_{1,3} + 2\hat{\mathbf{L}}_{1,2}^T \mathrm{B}_2 \hat{\mathbf{L}}_{1,3} \\ & + \hat{\mathbf{L}}_{1,3}^T \Sigma_2 \hat{\mathbf{L}}_{1,3} \\ \text{s.t.} \quad & 1 + \hat{\mathbf{L}}_{1,2}^T \hat{\mathbf{L}}_{1,2} = \hat{\mathbf{L}}_{1,3}^T \hat{\mathbf{L}}_{1,3} \end{aligned} \tag{13}$$

where the vector $\hat{\mathbf{L}}_{1,2}$ contains the second and the third element of $\hat{\mathbf{L}}_1$, $\hat{\mathbf{L}}_{1,3}$ contains the last three elements of $\hat{\mathbf{L}}_1$, σ_1 is the first element of Σ_1, Σ_1' is the lower right 2×2 submatrix of Σ_1, the vector $\mathbf{B}_1$ is the first row of B, the matrix B_2 is the last two rows of B. By the Lagrange's multiplier method, the Lagrange's function of criterion (13) can be formulated as

$$\begin{aligned} F = {} & \sigma_1 + \hat{\mathbf{L}}_{1,2}^T \Sigma_1' \hat{\mathbf{L}}_{1,2} + 2\mathbf{B}_1 \hat{\mathbf{L}}_{1,3} + 2\hat{\mathbf{L}}_{1,2}^T \mathrm{B}_2 \hat{\mathbf{L}}_{1,3} \\ & + \hat{\mathbf{L}}_{1,3}^T \Sigma_2 \hat{\mathbf{L}}_{1,3} + \lambda(1 + \hat{\mathbf{L}}_{1,2}^T \hat{\mathbf{L}}_{1,2} - \hat{\mathbf{L}}_{1,3}^T \hat{\mathbf{L}}_{1,3}) \end{aligned} \tag{14}$$

and the Lagrange's equations are

$$\begin{cases} \dfrac{\partial F}{\partial (\hat{\mathbf{L}}_{1,2}^T, \hat{\mathbf{L}}_{1,3}^T)^T} = \mathrm{M} \begin{pmatrix} \hat{\mathbf{L}}_{1,2} \\ \hat{\mathbf{L}}_{1,3} \end{pmatrix} + \begin{pmatrix} 0 \\ \mathbf{B}_1^T \end{pmatrix} = 0 \\ \dfrac{\partial F}{\partial \lambda} = 1 + \hat{\mathbf{L}}_{1,2}^T \hat{\mathbf{L}}_{1,2} - \hat{\mathbf{L}}_{1,3}^T \hat{\mathbf{L}}_{1,3} = 0 \end{cases} \tag{15}$$

Fig. 2 (*Continued*)

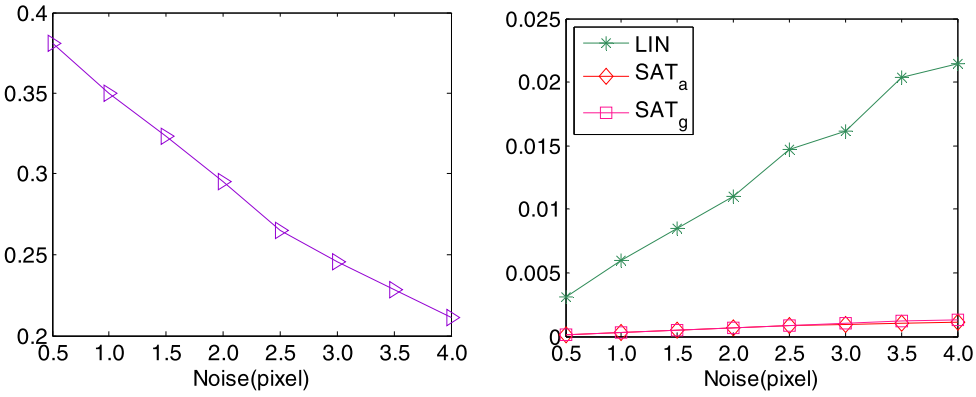

3 cameras, 2 degrees

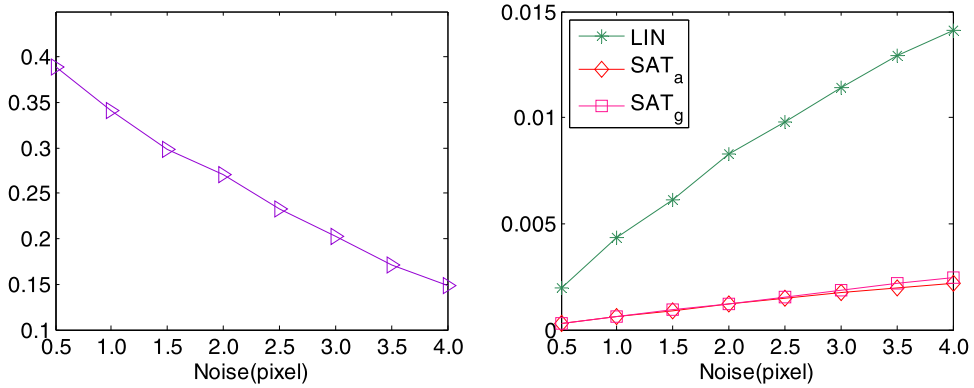

5 cameras, 2 degrees

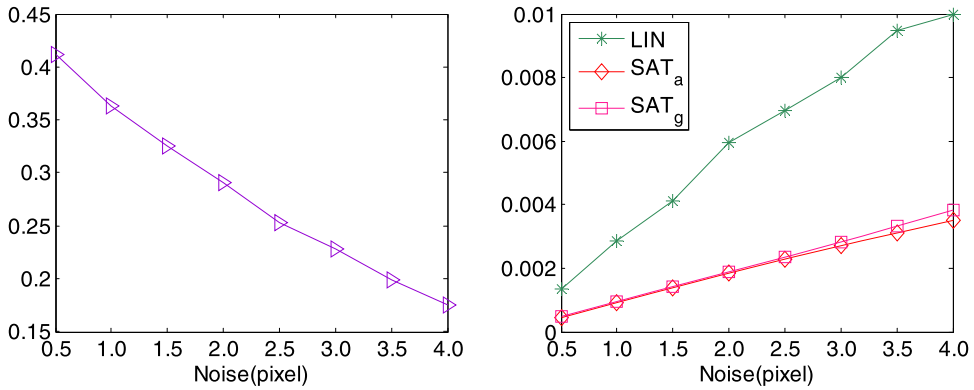

9 cameras, 2 degrees

where

$$\mathrm{M} = \begin{pmatrix} \Sigma_1' + \lambda \mathrm{I}_2 & \mathrm{B}_2 \\ \mathrm{B}_2^T & \Sigma_2 - \lambda \mathrm{I}_3 \end{pmatrix},$$

I_2 is the 2×2 identity matrix.

Suppose the determinant of M is nonzero, i.e. matrix M is invertible, then $(\hat{\mathbf{L}}_{1,2}^T, \hat{\mathbf{L}}_{1,3}^T)^T$ can be computed by the first equation of (15)

$$\begin{pmatrix} \hat{\mathbf{L}}_{1,2} \\ \hat{\mathbf{L}}_{1,3} \end{pmatrix} = \frac{\mathrm{M}^*}{\det(\mathrm{M})} \begin{pmatrix} 0 \\ -\mathbf{B}_1^T \end{pmatrix} \tag{16}$$

where M^* and $\det(\mathrm{M})$ are the adjoint matrix and the determinant of M, respectively. By substituting (16) into the second equation of (15), we obtain the following equation of λ

$$1 + \frac{(0^T \mathbf{B}_1)\mathrm{M}_1^{*T}\mathrm{M}_1^*\begin{pmatrix} 0 \\ \mathbf{B}_1^T \end{pmatrix}}{\det(\mathrm{M})^2} - \frac{(0^T \mathbf{B}_1)\mathrm{M}_2^{*T}\mathrm{M}_2^*\begin{pmatrix} 0 \\ \mathbf{B}_1^T \end{pmatrix}}{\det(\mathrm{M})^2} = 0$$

or equivalently

$$\det(\mathrm{M})^2 + (0^T \mathbf{B}_1)\mathrm{M}_1^{*T}\mathrm{M}_1^* \begin{pmatrix} 0 \\ \mathbf{B}_1^T \end{pmatrix} - (0^T \mathbf{B}_1)\mathrm{M}_2^{*T}\mathrm{M}_2^* \begin{pmatrix} 0 \\ \mathbf{B}_1^T \end{pmatrix} = 0 \tag{17}$$

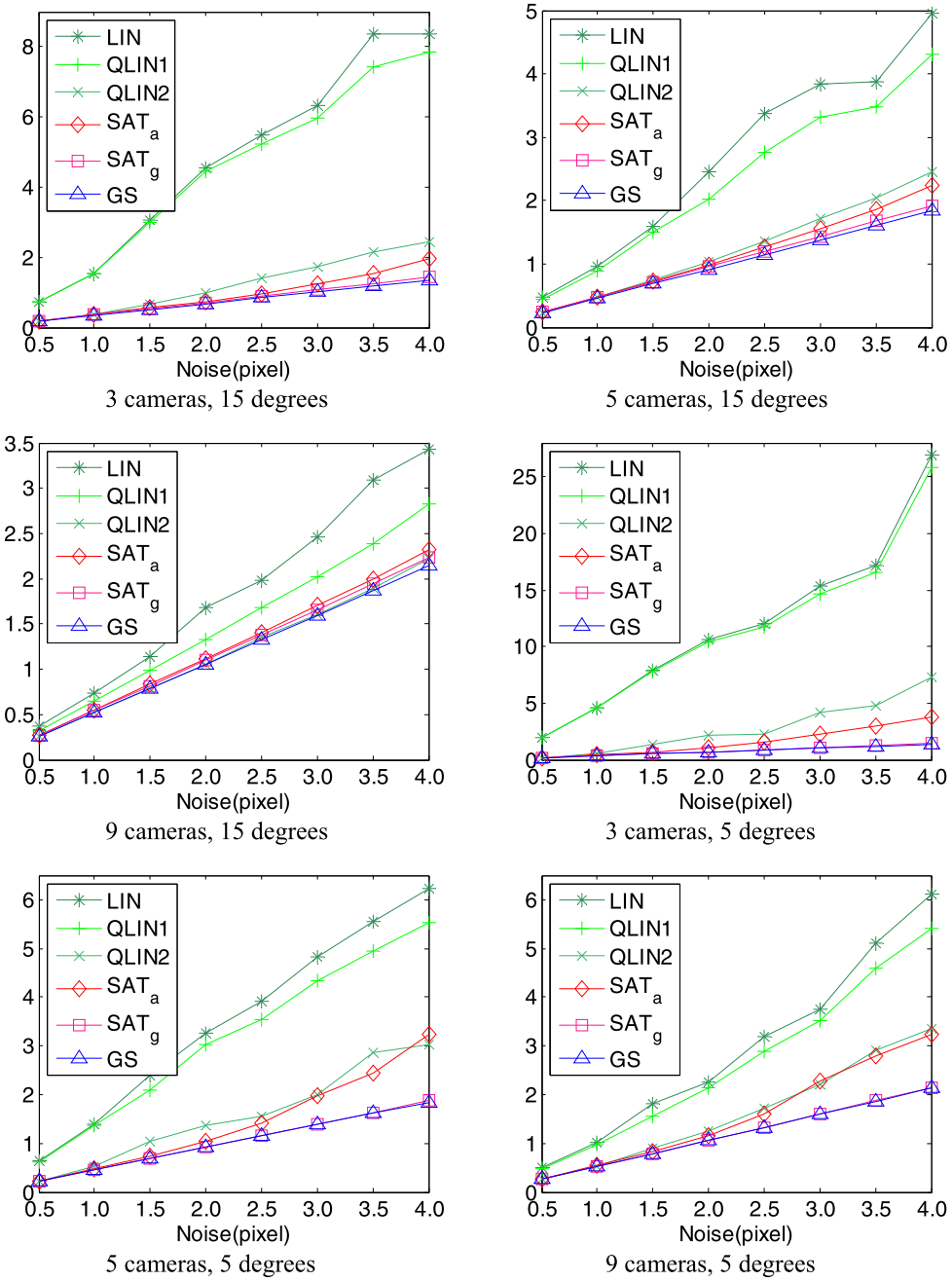

Fig. 3 Experimental results of the Configuration I. RMS of geometric error (pixel)

where matrices M_1^* and M_2^* are the first two rows and last three rows of M^*, respectively. Equation (17) is a 10-degree polynomial equation in λ, the companion matrix method is used here to solve it. The coefficients of λ in (17) can be obtained from $\det(\mathrm{M}), \mathrm{M}_1^*, \mathrm{M}_2^*$ as shown in Appendix A. From the roots of Eq. (17), the real roots which do not make $\det(\mathrm{M}) = 0$ are selected to compute the candidates of $(\hat{\mathbf{L}}_{1,2}^T, \hat{\mathbf{L}}_{1,3}^T)^T$ by (16).

Next, we consider the case that the determinant of M is zero. When $\det(\mathrm{M}) = 0$, 5 roots, λ_i $(i = 1, \ldots, 5)$, can be computed by the companion matrix method. By substituting λ_i into M, the eigen-decomposition of the matrix $\mathrm{M}(\lambda_i)$ can be computed as:

$$\mathrm{M}(\lambda_i) = \mathrm{U}_i \begin{pmatrix} 0_{m_i} & 0 \\ 0 & \Sigma_{5-m_i} \end{pmatrix} \mathrm{U}_i^T,$$

where 0_{m_i} is the $m_i \times m_i$ zero matrix, Σ_{5-m_i} $(1 \leq m_i \leq 4)$ is a $(5 - m_i) \times (5 - m_i)$ diagonal matrix. Note that the matrix U_i in the decomposition is not uniquely defined, however, such a nonuniqueness has no effect on the subsequent computing process. Then, the first polynomial equation of (15)

Fig. 3 (*Continued*)

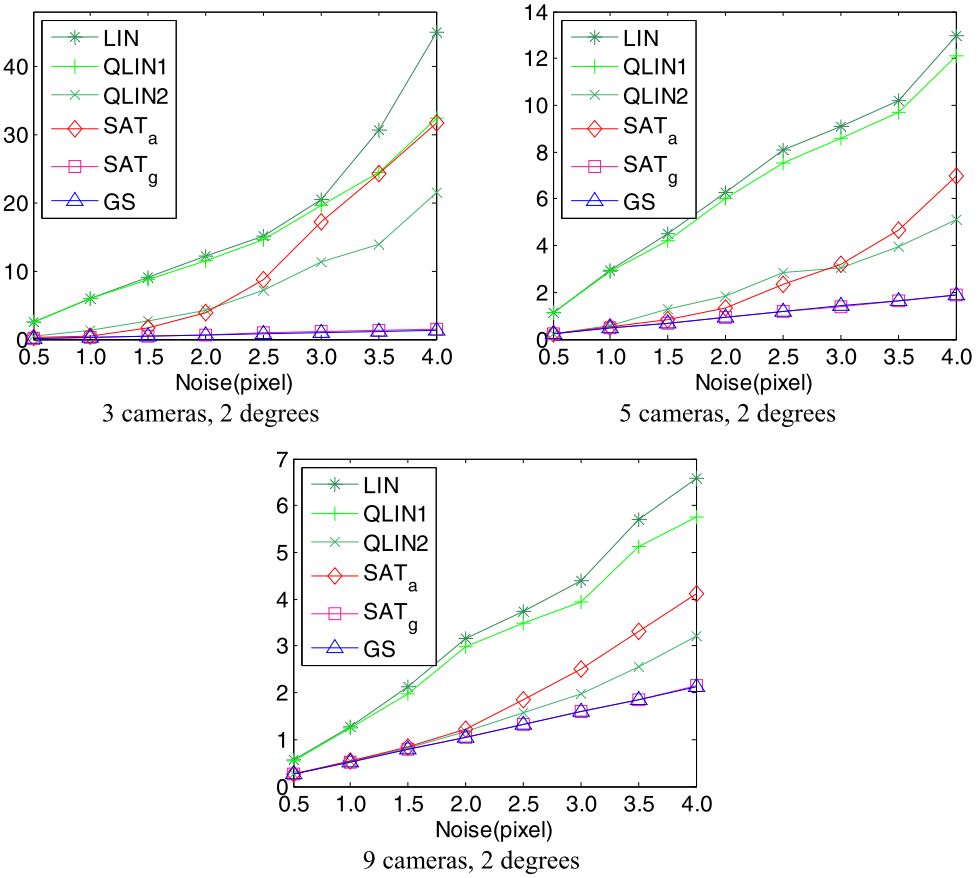

can be rewritten as

$$\begin{pmatrix} 0_{m_i} & 0 \\ 0 & \Sigma_{5-m_i} \end{pmatrix} \mathrm{U}_i^T \begin{pmatrix} \hat{\mathbf{L}}_{1,2} \\ \hat{\mathbf{L}}_{1,3} \end{pmatrix} = \mathrm{U}_i^T \begin{pmatrix} 0 \\ -\mathbf{B}_1^T \end{pmatrix} \tag{18}$$

Obviously, Eq. (18) can be solved iff all the first m_i elements of the vector $\mathrm{U}_i^T \begin{pmatrix} 0 \\ -\mathbf{B}_1^T \end{pmatrix}$ are zeros. If this condition is satisfied, we can use the method in Appendix B to obtain the candidates of $(\hat{\mathbf{L}}_{1,2}^T, \hat{\mathbf{L}}_{1,3}^T)^T$; otherwise, there is no candidate of $(\hat{\mathbf{L}}_{1,2}^T, \hat{\mathbf{L}}_{1,3}^T)^T$ in the case of $\det(\mathrm{M}) = 0$.

By evaluating the cost function in (13) at all the candidates of $(\hat{\mathbf{L}}_{1,2}^T, \hat{\mathbf{L}}_{1,3}^T)^T$, the optimal solution $\hat{\mathbf{L}}_1^{opt}$ of (13), which gives the smallest value of the cost function, is selected and its original-space solution $\bar{\mathbf{L}}_1^{opt}$ can be computed via normalization and the inverse transformation (10).

6 Experiments

The experiments are carried out to evaluate six different algorithms using MATLAB on a PC with Intel Core i5 3.2 GHz CPU and 4 GB RAM. These six compared algorithms include: LIN (linear algorithm [15]), QLIN1 and QLIN2 (two quasi-linear algorithms [15]), $\mathrm{SAT_a}$(suboptimal algebraic-error triangulation with the algebraic suboptimal solution), $\mathrm{SAT_g}$(suboptimal algebraic-error triangulation with the geometric suboptimal solution), and GS (Gold Standard algorithm [19] which minimizes the geometric error), where the GS provides the benchmark of estimation accuracy. In the GS, we choose the coordinates of lines in two furthest cameras as the estimated parameters and obtain the coordinates of the other lines with the trifocal tensors of corresponding triple views. The initial values of the estimated parameters are obtained by the measured lines in two cameras whose corresponding 3D line has the smallest geometric error and the time of finding the initial values is not included in the time cost of the GS.

In our experiments, two typical camera configurations are considered:

Configuration I (Circular configuration) As shown in Fig. 1 (left), the endpoints of observed lines lie in a sphere (dotted line) whose center is O and radius is 2 units. The nine cameras' optical axes pass through the center O and their centers lie on the same circle centered at O with fixed radius 11 units. The angles between the optical axes of adjacent cameras (called the optical-axis angle) are set to the same value. Camera A, B and C are utilized in the three-camera experiments. In the five-camera and the nine-camera experiment, camera A, B, C, D, E and all the nine cameras are utilized, respectively. The optical-axis angle is

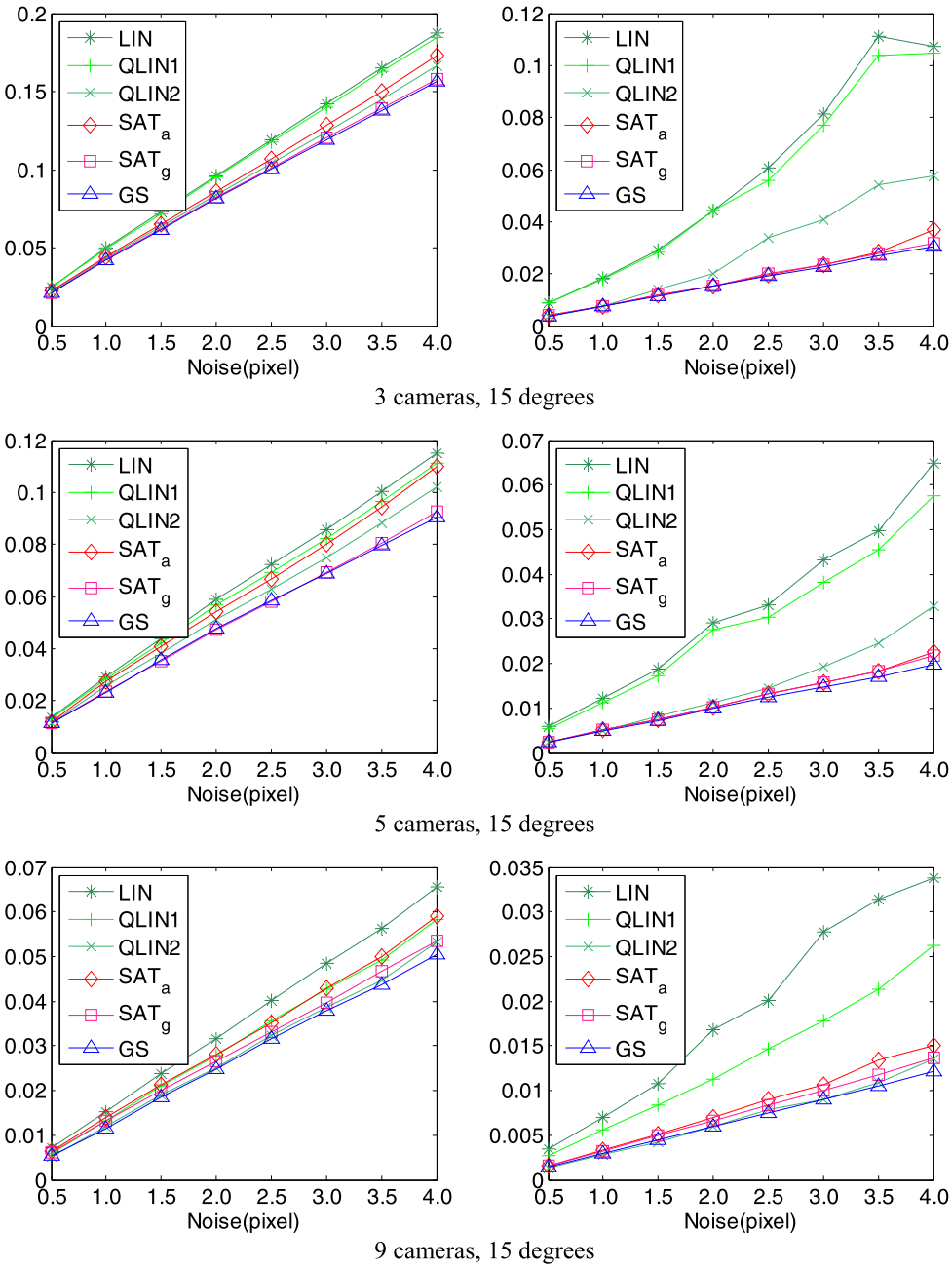

Fig. 4 Experimental results of the Configuration I. (*Left*)Average error of space angle (radian). (*Right*) RMS error of space distance (unit)

respectively set to 15, 5 and 2 degrees in all three experiments.

Configuration II (Radial configuration) As shown in Fig. 1 (right), a sphere (dotted line) with center O and radius 2 units contains the endpoints of all observed lines. Camera is moved along a ray towards the center O and the distance of each movement (called the each-movement distance) is fixed at the same value. The distance between the center O and the initial position of camera is 11 units. The three-camera experiments and the five-camera experiments are utilized to evaluate the performances of the six algorithms, in which camera is moved twice and four times, respectively. The each-movement distance is respectively set to 2, 1 and 0.2 units in both experiments.

Under each of the two configurations, the internal matrices of the cameras are set as:

$$\mathrm{K} = \begin{pmatrix} 700 & 0 & 512 \\ 0 & 700 & 512 \\ 0 & 0 & 1 \end{pmatrix}.$$

In each of our experiments, the cameras' centers are slightly perturbed to simulate the situation in real practice. 200 observed lines are randomly chosen and projected onto 1024×1024 image plane. For each image line, 8 random points

Fig. 4 (*Continued*)

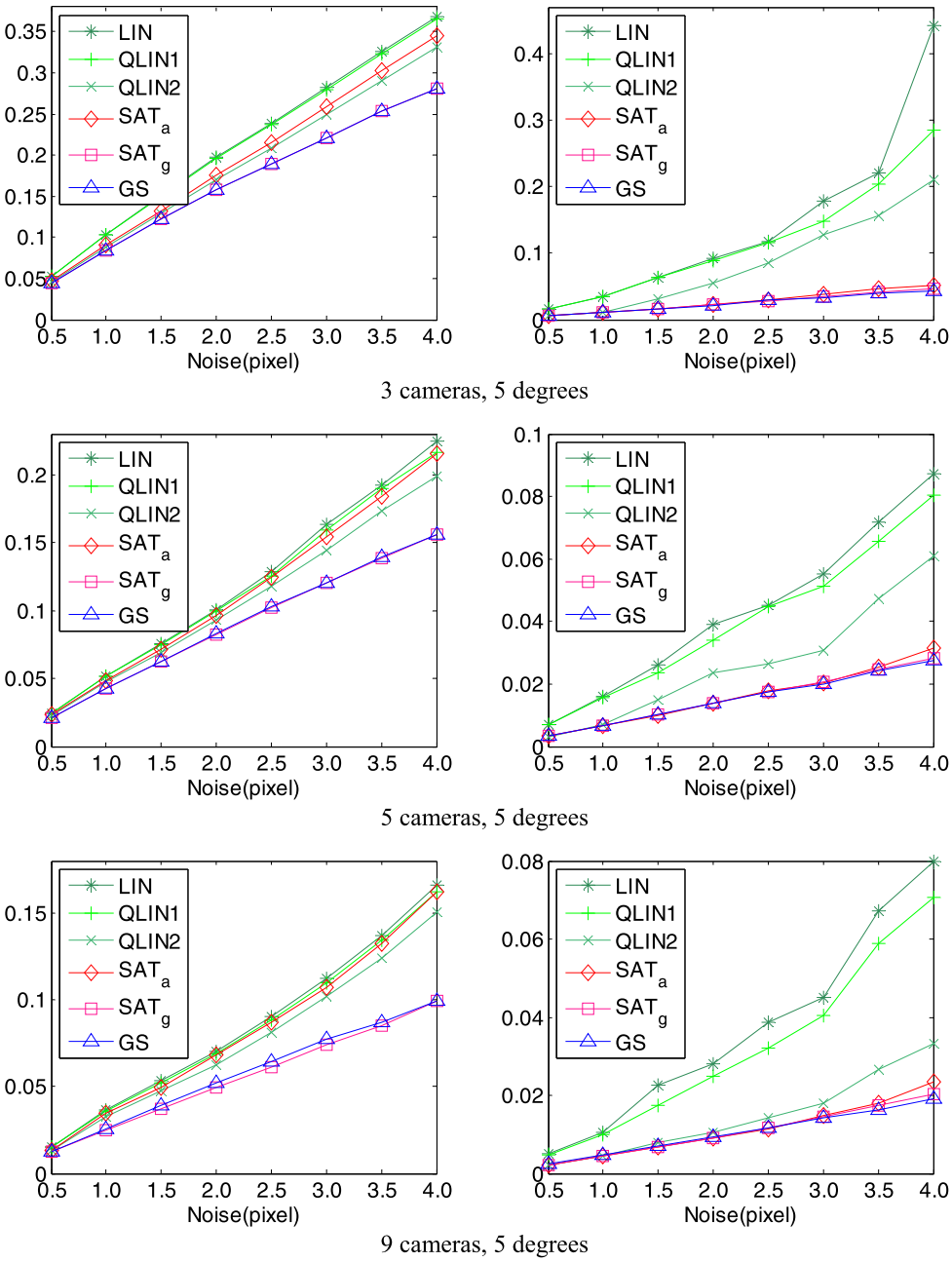

on it and 2 endpoints are corrupted by Gaussian noise with zero mean and standard deviation σ. Then, the measured line is fitted with all the 10 noisy points by the least-squares method and the measured endpoints are chosen as the closest points on the measured line to the noisy endpoints. The noise level σ varies from 0.5 to 4 with the steps of 0.5 pixels, 200 trials are performed at each noise level to obtain the statistically meaningful experimental results. The evaluated performances include: Result repeat ratio of the SAT_a and the SAT_g which is the ratio of the trials with the same results by them to the total trials; RMS of algebraic error of the LIN, the SAT_a and the SAT_g; RMS of geometric error; Average error of space angle which is the acute angle between the tangent vectors of the observed line and the estimated line in space [20]; RMS error of space distance which is the closest Euclidean distance between the observed line and the estimated line in space; Average of running time.

6.1 Experimental Results of the Configuration I

Experimental results for the Configuration I are shown in Figs. 2, 3, 4 and 5. Figure 2 (left) shows the result repeat ratios of the SAT_a and the SAT_g. From Fig. 2 (left), we can see that the repeat ratios are not more than 55 % for all the experiments and their curves decline more rapidly with the

Fig. 4 (*Continued*)

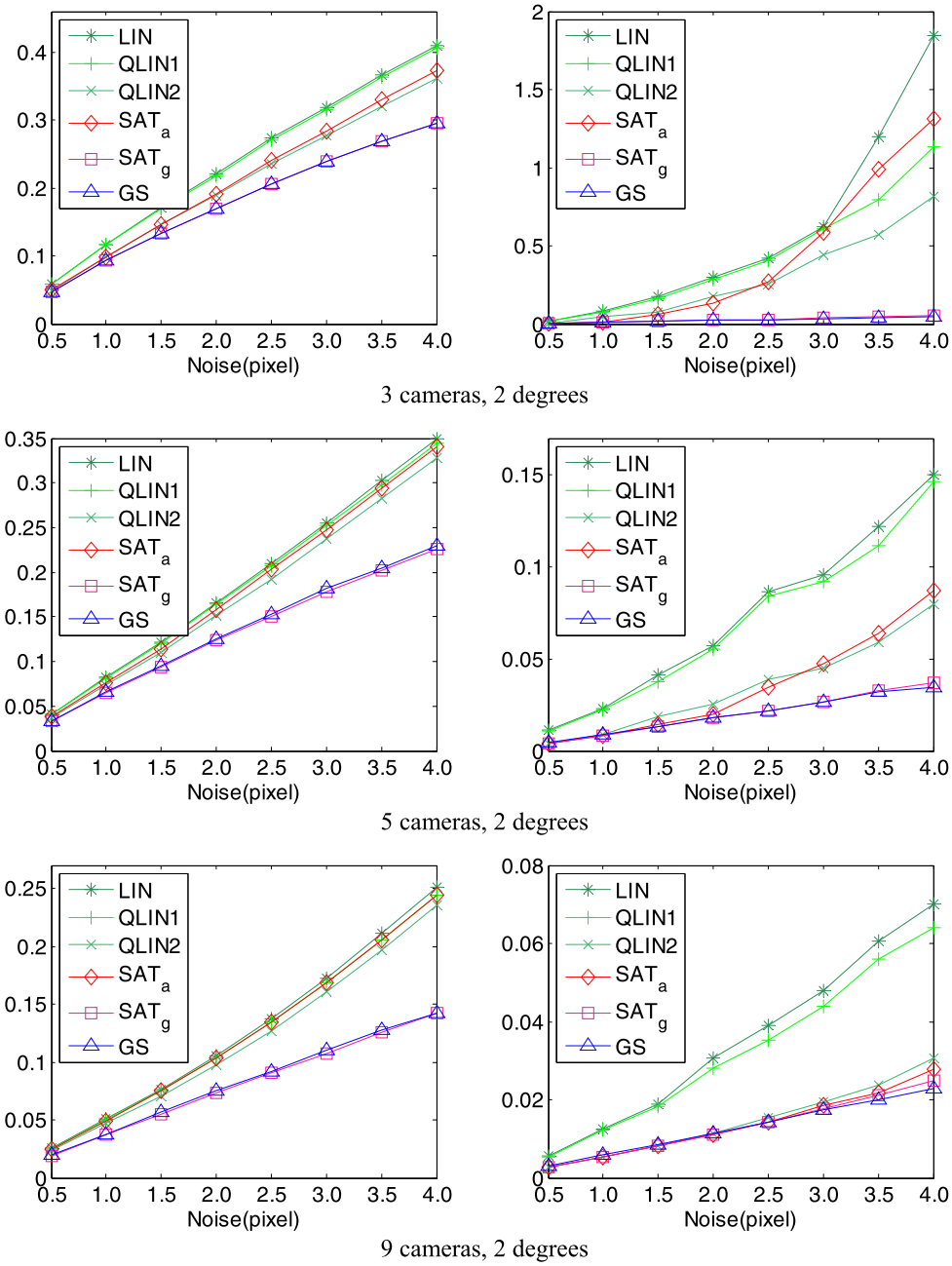

decrease of the optical-axis angle. However, for the RMS of algebraic error (Fig. 2 (right)), it can be seen the SAT_g manifests little difference to the SAT_a compared with the LIN. Figure 3 shows the RMS of geometric error. We can see that: in all the experiments both the LIN and the QLIN1 have large RMS errors; the RMS error curves of the SAT_g are much close to those of the GS and the differences between their RMS errors are not more than 0.1 pixels; the RMS errors of the SAT_a and the QLIN2 increase significantly with the increase of measurement error when the optical-axis angles are 5 degrees and 2 degrees, but when measurement error is less than 2 pixels the RMS error increase of the SAT_a in most cases is not more than that of the QLIN2 whose initial value is the solution of the LIN.

Figure 4 shows the average error of space angle and the RMS error of space distance. These results indicate that, for the space angle and the space distance, the LIN has the worst estimation accuracy among all the algorithms, whereas the SAT_g has comparable estimation accuracy with the GS and both their estimation accuracies are better than those of the other four algorithms. For the other three algorithms, from Fig. 4 (left) it can be seen that, the space angle errors of the SAT_a are between those of the QLIN2 and the QLIN1, and are close to those of the QLIN2 with the decrease of

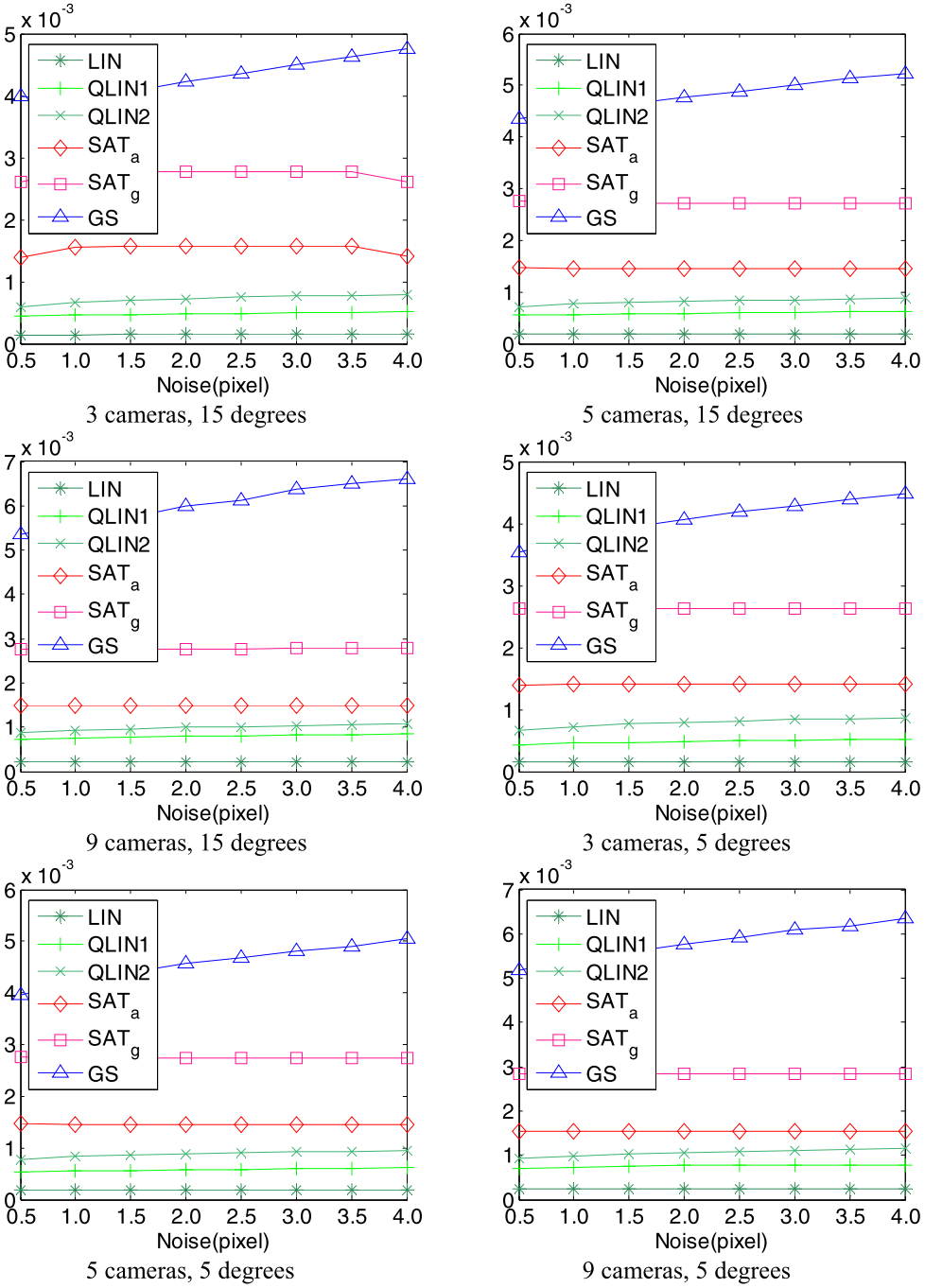

Fig. 5 Experimental results of the Configuration I. Average of running time (second)

the number of cameras; from Fig. 4 (right) it can be seen that, although for a near-degenerative configuration, such as the optical-axis angle equal to 2 degrees, the space distance errors of the SAT_a become worse than those of the QLIN2 and even worse than those of the QLIN1 with the decrease of the number of cameras, the SAT_a has comparable space distance error with the GS when the optical-axis angle are 15 degrees or 5 degrees. Figure 5 shows the time costs of the six algorithms. It is obvious that the time costs of the GS are the largest and increase with the increase of the number of cameras, the increase of the measurement error and the increase of the optical-axis angle. Conversely, the time costs of the other five algorithms do not change with any increases mentioned above.

6.2 Experimental Results of the Configuration II

Experimental results of the Configuration II are shown in Figs. 6, 7, 8, and 9, which are similar to those of the Configuration I. Here, we just give some discussions on the estimation accuracy and the time cost as shown in Figs. 8 and 9.

Fig. 5 (*Continued*)

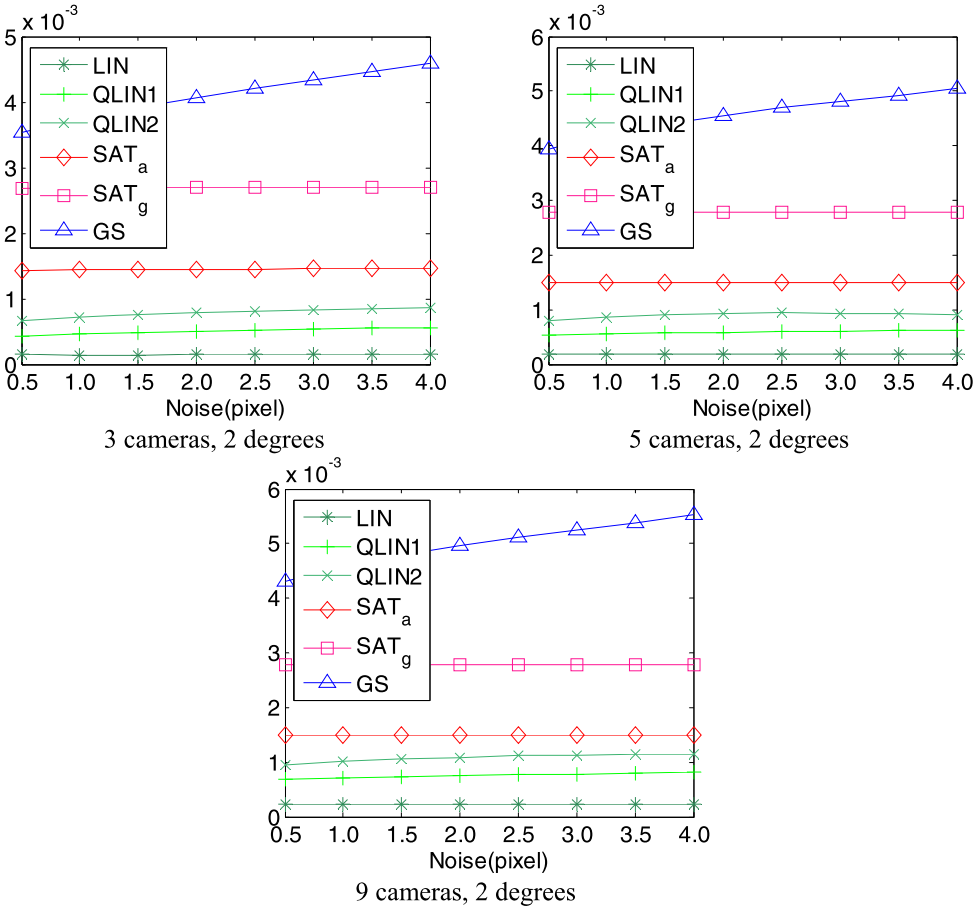

For the SAT_g, from Fig. 8, we can see that it has almost the same estimation accuracy with the GS, but its time costs are less than those of the GS as shown in Fig. 9. For the SAT_a, although its performance become much worse with the increase of measurement error in the near-degenerative configuration whose each-movement distance is 0.2 units, its space angle errors are close to those of the QLIN2 and its distance errors are less than those of the QLIN2 when the each-movement distances are 2 units and 1 unit; moreover, its time costs shown in Fig. 9 are slightly more than those of the QLIN2. In Fig. 9, the time costs of the LIN and the QLIN1 are less than those of the other four algorithms, but their bad performances disqualify them for any real applications in practice.

In addition, through the comparison of space angle errors and space distance errors in different experiments, it is shown that the number of cameras and the optical-axis angle (or the each-movement distance) are important factors to affect the estimation accuracy. And from all these experiments in both the configurations, we find that Eq. (18) in Sect. 5 is always unsolvable, which means that both the suboptimal solutions are obtained just via the solving process in the case of $\det(M) \neq 0$.

7 Conclusions

This paper proposes two suboptimal algorithms for multiple-view algebraic-error line triangulation. The main contributions include: (1) Via transforming the Klein constraint and introducing a set of linear constraints, six new single-quadric-constraint optimality criteria are proposed; (2) In the transformed solution space, we prove that the upper bound of the smallest algebraic error from only three of the six new criteria is just $\sqrt{3}$ times of the minimum algebraic error of the original optimality criterion; (3) Via converting the new criteria to polynomial equations, two suboptimal solutions are obtained by non-iterative method. Experimental results show that our suboptimal solutions under the geometric error minimization always have smaller space angle errors and space distance errors than those under the algebraic error minimization. Thus, in our future work, we will focus on efficient geometric-error line triangulation.

Acknowledgements We wish to thank the anonymous reviewers for their inspiring comments and suggestions. Also, we gratefully acknowledge the support from the Open Project Program of the National Laboratory of Pattern Recognition (NLPR) (201204243), the Funda-

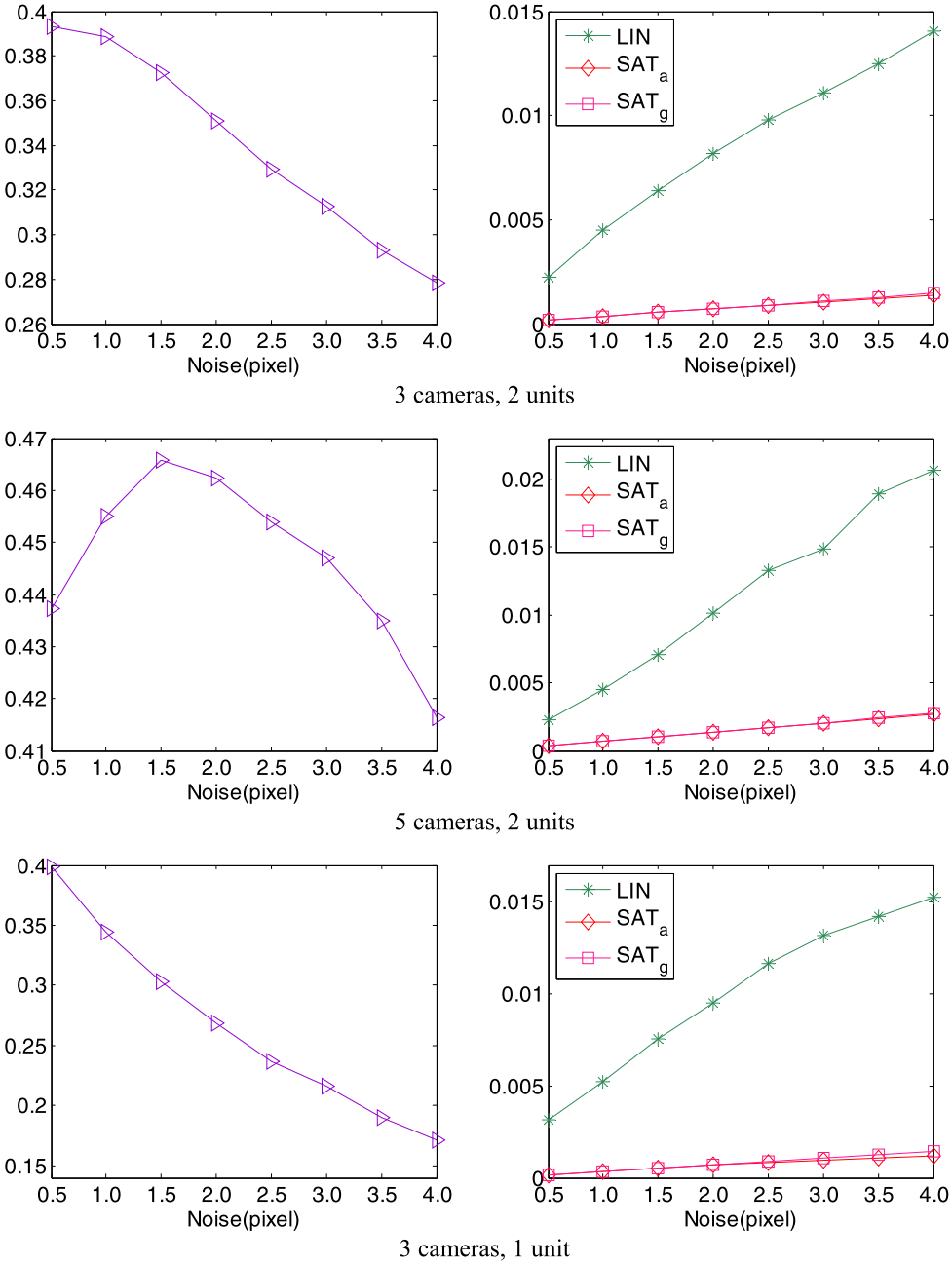

Fig. 6 Experimental results of the Configuration II. (*Left*) Result repeat ratio of the $\mathrm{SAT_a}$ and the $\mathrm{SAT_g}$. (*Right*) RMS of algebraic error of the LIN, the $\mathrm{SAT_a}$ and the $\mathrm{SAT_g}$

mental Research Funds for the Central Universities (K5051302009), the Natural Science Foundation of China (Nos. 61272281, 61271297, 61375042), and the Specialized Research Fund for the Doctoral Program of Higher Education (No. 20110203110001).

Appendix A

For

$$\mathrm{M}(\lambda) = \begin{pmatrix} \Sigma_1' + \lambda \mathrm{I}_2 & \mathrm{B}_2 \\ \mathrm{B}_2^T & \Sigma_2 - \lambda \mathrm{I}_3 \end{pmatrix},$$

where λ is unknown, its determinant can be expanded as:

$$\begin{aligned} \det(\mathrm{M}) &= -\det\left(\begin{pmatrix} \Sigma_1' & -\mathrm{B}_2 \\ \mathrm{B}_2^T & -\Sigma_2 \end{pmatrix} + \lambda \mathrm{I}_n\right) \\ &= -\lambda^n - \sum_{i=1}^{n} \left[\begin{pmatrix} \Sigma_1' & -\mathrm{B}_2 \\ \mathrm{B}_2^T & -\Sigma_2 \end{pmatrix}\right]_i \lambda^{n-i} \end{aligned} \tag{19}$$

where $[\cdot]_i$ is the sum of all the $i \times i$ principal minors, I_n is the $n \times n$ identity matrix and n is the order of M. Then, from (17) we know that just the last three columns of the adjoint matrix of M are needed. So, here we just discuss the cofactors of the last three rows in M and there are three situations:

(1) Elements on the main diagonal: their cofactors can be obtained according to (19).

Fig. 6 (*Continued*)

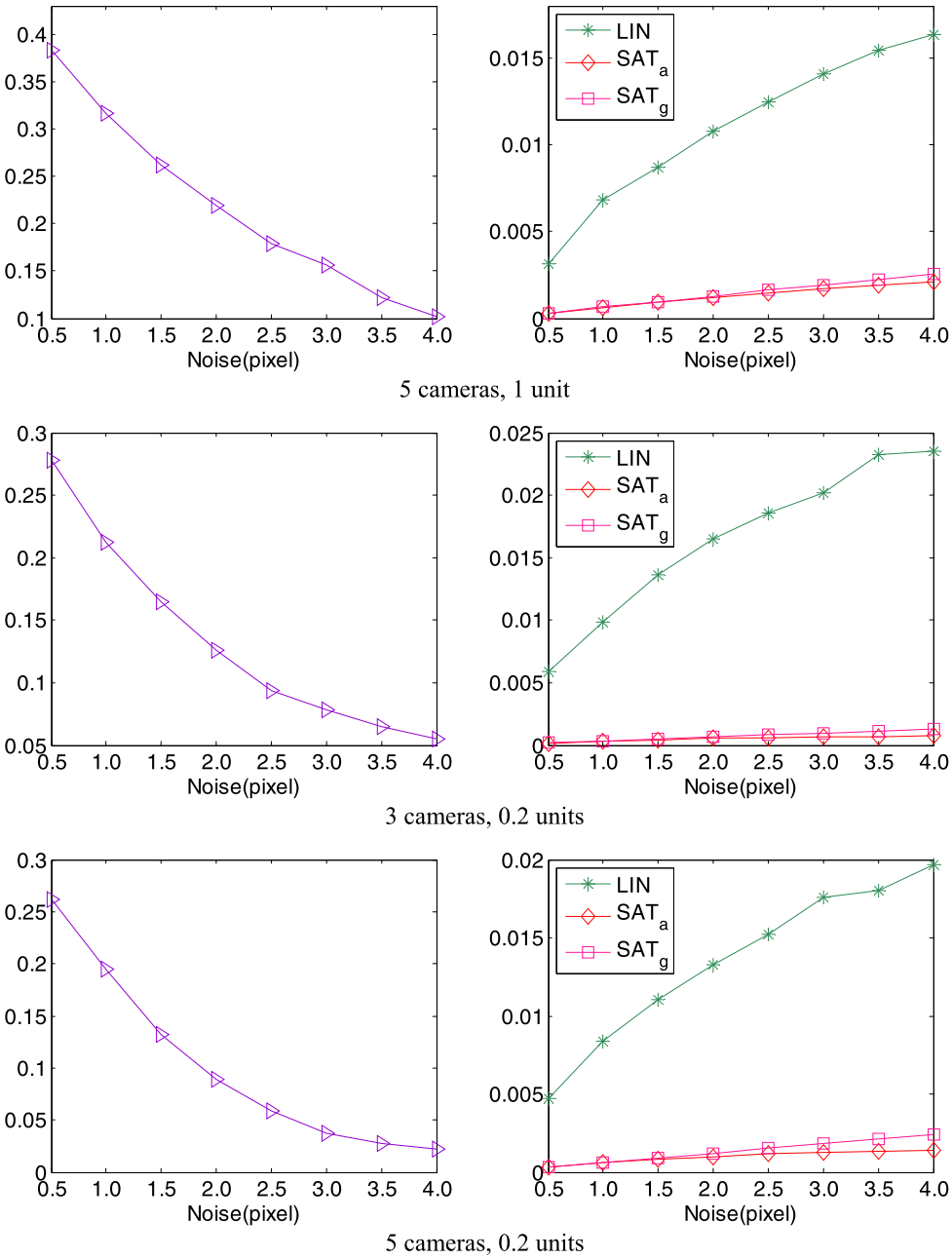

(2) Nonzero elements at the ith row and the jth column ($i \neq j$): their cofactors are the determinants of matrices like the following form, where the matrices are obtained by row or column exchanges of the submatrices formed by deleting the ith row and the jth column:

$$\begin{vmatrix} 0 & h_{12} & h_{13} & h_{14} \\ p+\lambda & h_{22} & h_{23} & h_{24} \\ h_{31} & 0 & q_1-\lambda & 0 \\ h_{41} & 0 & 0 & q_2-\lambda \end{vmatrix}$$

$$= -h_{12}\lambda^3 - h_{12}(p-q_1-q_2)\lambda^2 - (h_{12}h_{23}h_{31} + h_{12}h_{24}h_{41} + h_{12}q_1q_2 - h_{13}h_{22}h_{31} - h_{14}h_{22}h_{41} - h_{12}pq_1 - h_{12}pq_2)\lambda + h_{12}h_{24}h_{41}q_1 + h_{12}h_{23}h_{31}q_2 - h_{14}h_{22}h_{41}q_1 - h_{13}h_{22}h_{31}q_2 - h_{12}pq_1q_2$$

(3) Zero elements at the ith row and the jth column ($i \neq j$): their cofactors are the negative determinants of matrices like the following form, where the matrices are obtained by row or column exchanges of the submatices formed by deleting the ith row and the jth column:

$$\begin{vmatrix} p_1+\lambda & 0 & h_{13} & h_{14} \\ 0 & p_2+\lambda & h_{23} & h_{24} \\ h_{31} & h_{32} & 0 & 0 \\ h_{41} & h_{42} & 0 & q-\lambda \end{vmatrix}$$

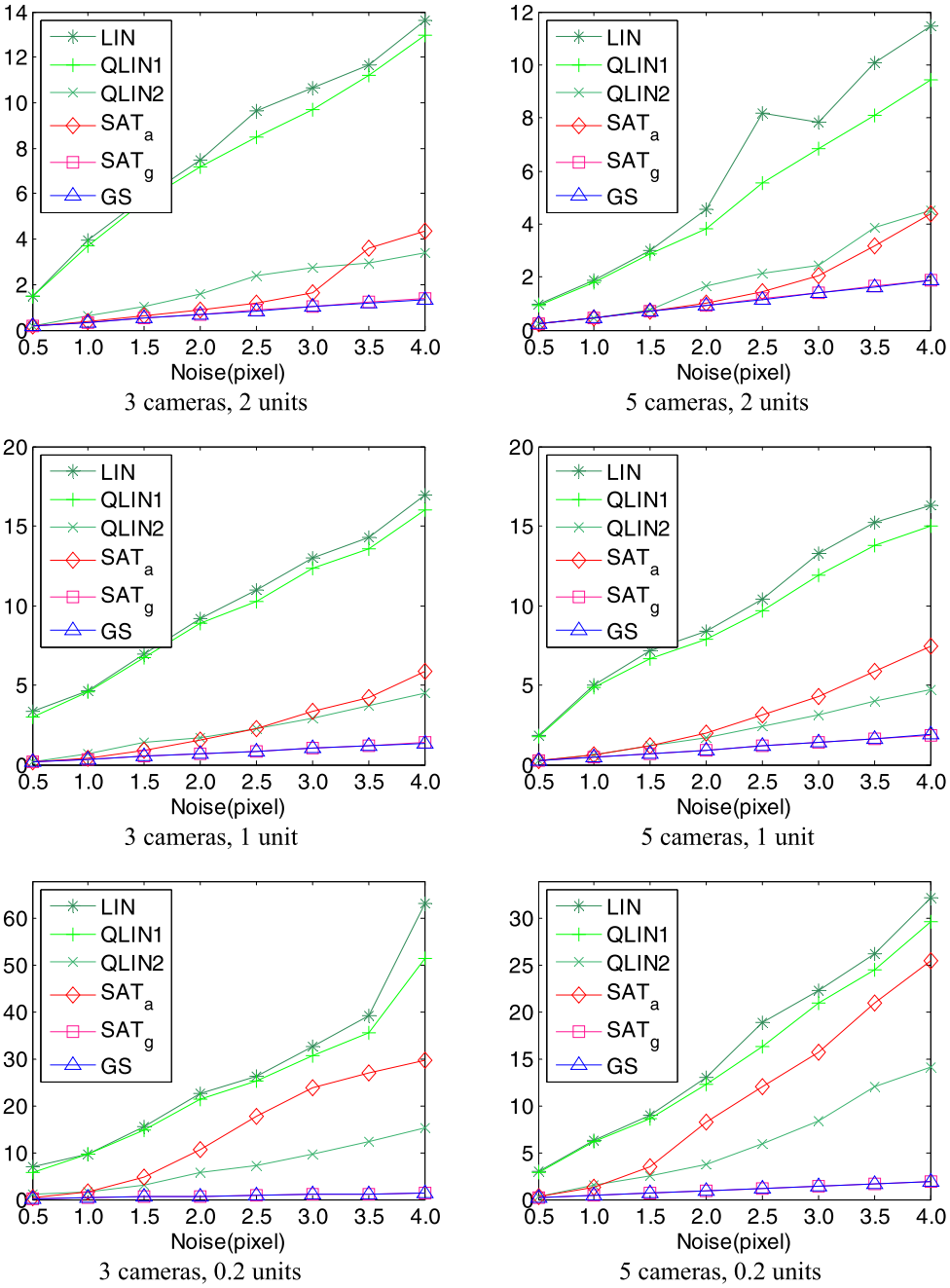

Fig. 7 Experimental results of the Configuration II. RMS of geometric error (pixel)

$$
\begin{aligned}
&= (h_{13}h_{31} + h_{23}h_{32})\lambda^2 \\
&\quad + (h_{23}h_{32}p_1 + h_{13}h_{31}p_2 - h_{13}h_{31}q - h_{23}h_{32}q)\lambda \\
&\quad + h_{14}h_{23}h_{32}h_{41} + h_{13}h_{24}h_{31}h_{42} - h_{13}h_{24}h_{32}h_{41} \\
&\quad - h_{14}h_{23}h_{31}h_{42} - h_{23}h_{32}p_1q - h_{13}h_{31}p_2q
\end{aligned}
$$

Appendix B

If the first m_i elements in $\mathrm{U}_i^T \begin{pmatrix} 0 \\ -\mathbf{B}_1^T \end{pmatrix}$ are zero, we discuss how to compute the candidates of $(\hat{\mathbf{L}}_{1,2}^T, \hat{\mathbf{L}}_{1,3}^T)^T$ from the following two situations.

B.1 Situation $m_i = 1$

$$
\begin{pmatrix} \hat{\mathbf{L}}_{1,2} \\ \hat{\mathbf{L}}_{1,3} \end{pmatrix} = \mathrm{U}_i \begin{pmatrix} \mu_i \\ \mathbf{v}_i \end{pmatrix} \tag{20}
$$

where μ_i is an unknown, $\mathbf{v}_i = (0 \ \ \Sigma_4^{-1})\mathrm{U}_i^T \begin{pmatrix} 0 \\ -\mathbf{B}_1^T \end{pmatrix}$ is a constant vector. Substituting (20) into the second equation in (15), we obtain a quadratic equation. The candidates of $(\hat{\mathbf{L}}_{1,2}^T, \hat{\mathbf{L}}_{1,3}^T)^T$ can be obtained by real roots of the quadratic equation.

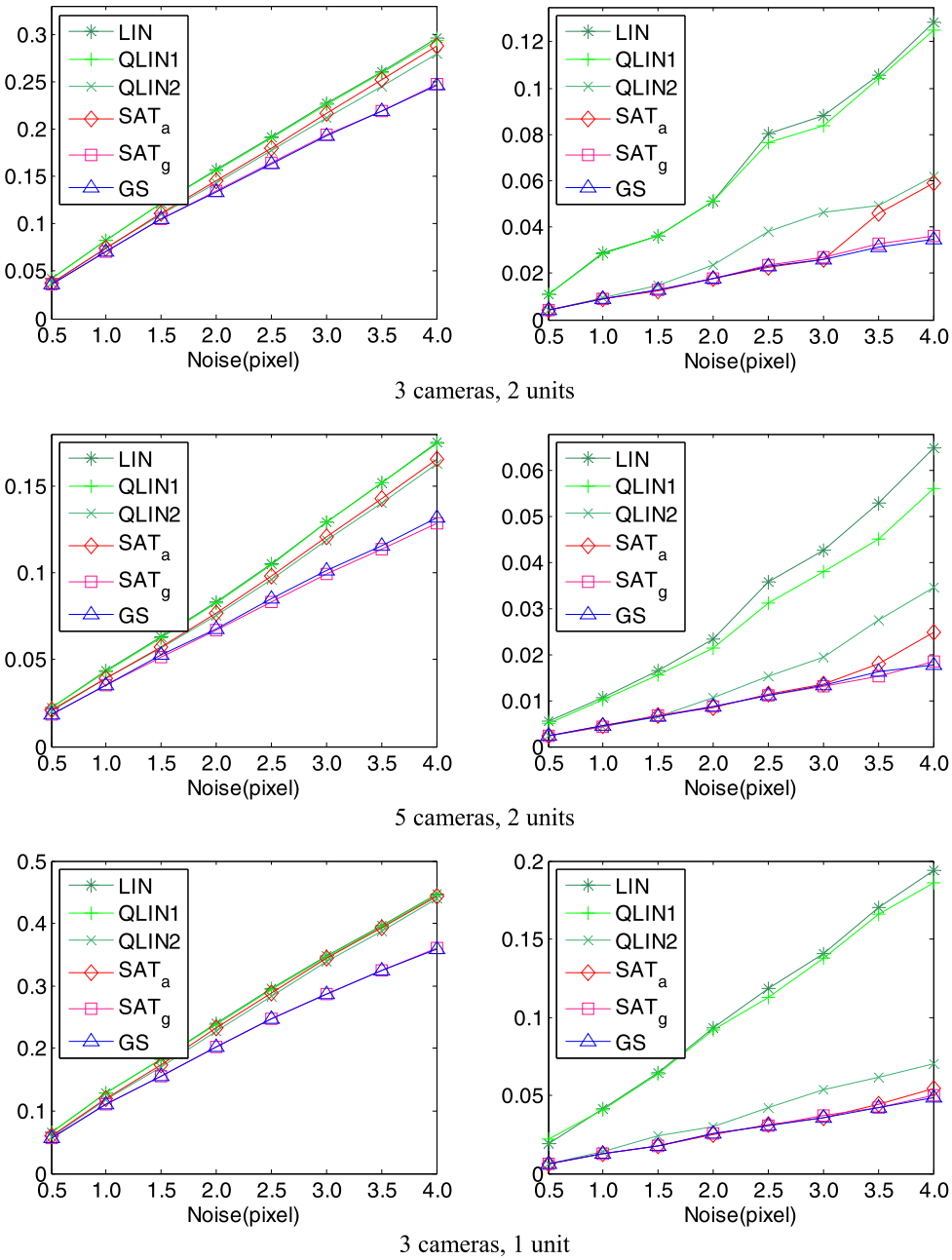

Fig. 8 Experimental results of the Configuration II. (*Left*) Average error of space angle (radian). (*Right*) RMS error of space distance (unit)

B.2 Situation $m_i > 1$

$$\begin{pmatrix} \hat{\mathbf{L}}_{1,2} \\ \hat{\mathbf{L}}_{1,3} \end{pmatrix} = \mathrm{U}_i \begin{pmatrix} \boldsymbol{\mu}_i \\ \mathbf{v}_i \end{pmatrix} \tag{21}$$

where $\boldsymbol{\mu}_i$ is an m_i-dimensional unknown vector, $\mathbf{v}_i = (0\ \ \Sigma_{5-m_i}^{-1})\mathrm{U}_i^T \begin{pmatrix} 0 \\ -\mathbf{B}_1^T \end{pmatrix}$ is a constant vector when $m_i \leq 3$ or a constant when $m_i = 4$. Substituting (21) into the second equation in (15), a quadratic equation of m_i variants is obtained, which has infinitely many solutions. To reduce the number of the candidates of $(\hat{\mathbf{L}}_{1,2}^T, \hat{\mathbf{L}}_{1,3}^T)^T$ from the quadratic equation, we select the candidate that gives the smallest value of the cost function in (13), which is equivalent to the optimal solution to the minimization problem of m_i-vector $\boldsymbol{\mu}_i$ constructed by substituting (21) into the criterion (13)

$$\begin{aligned} \min_{\boldsymbol{\mu}_i} \quad & (\boldsymbol{\mu}_i^T, \mathbf{v}_i^T, 1)\mathrm{D} \begin{pmatrix} \boldsymbol{\mu}_i \\ \mathbf{v}_i \\ 1 \end{pmatrix} \\ \text{s.t.} \quad & (\boldsymbol{\mu}_i^T, \mathbf{v}_i^T, 1)\mathrm{S} \begin{pmatrix} \boldsymbol{\mu}_i \\ \mathbf{v}_i \\ 1 \end{pmatrix} = 0 \end{aligned}$$

or equivalently

$$\begin{aligned} \min \quad & \boldsymbol{\mu}_i^T \mathrm{D}_{11} \boldsymbol{\mu}_i + 2\mathbf{d}_1 \boldsymbol{\mu}_i + d_2 \\ \text{s.t.} \quad & \boldsymbol{\mu}_i^T \mathrm{S}_{11} \boldsymbol{\mu}_i + 2\mathbf{s}_1 \boldsymbol{\mu}_i + s_2 = 0 \end{aligned} \tag{22}$$

Fig. 8 (*Continued*)

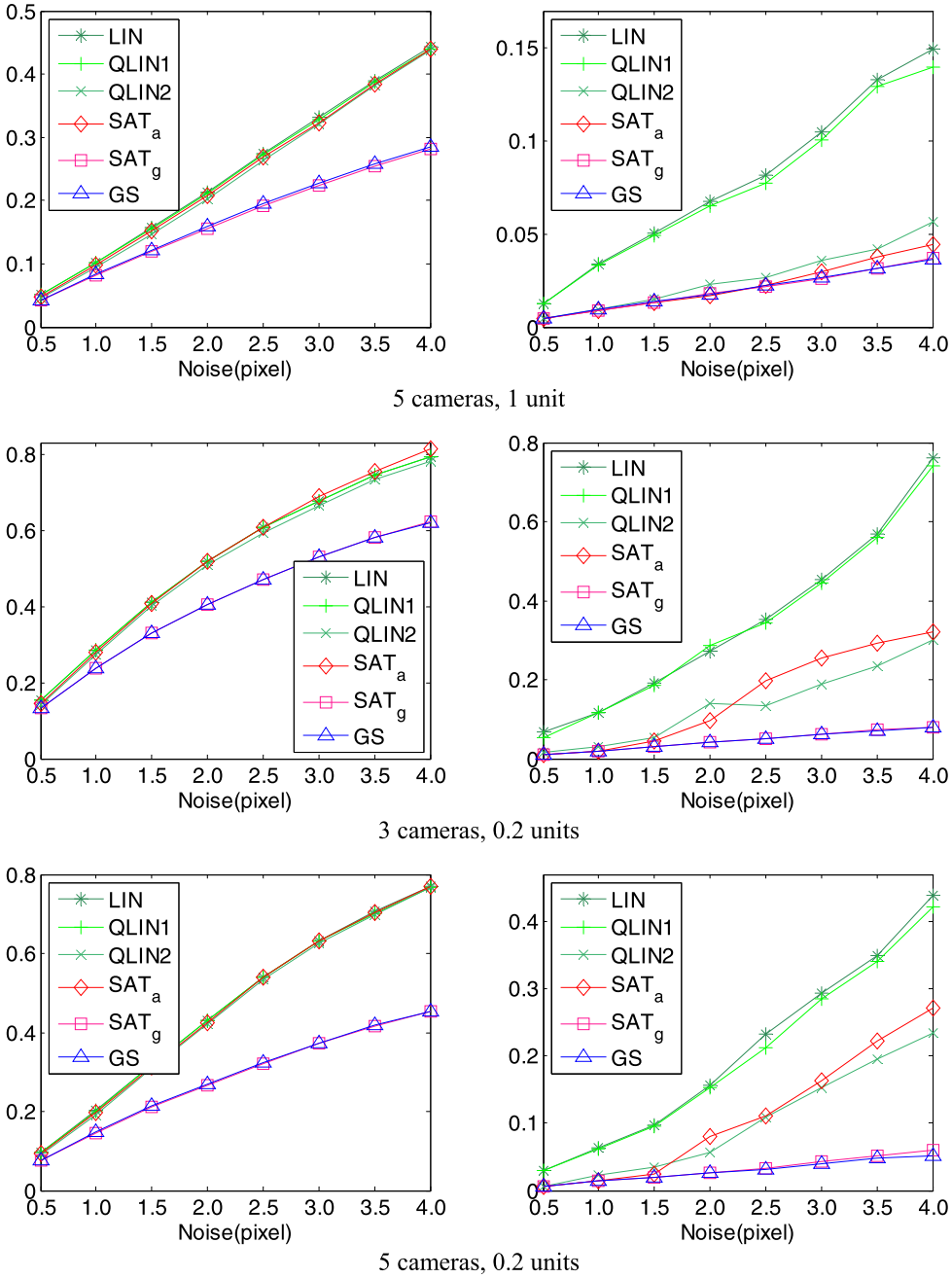

where

$$\mathrm{D}=\begin{pmatrix}\mathrm{U}_i^T & 0\\ 0 & 1\end{pmatrix}\begin{pmatrix}\Sigma_1' & \mathrm{B}_2 & 0\\ \mathrm{B}_2^T & \Sigma_2 & \mathbf{B}_1^T\\ 0 & \mathbf{B}_1 & \sigma_1\end{pmatrix}\begin{pmatrix}\mathrm{U}_i & 0\\ 0 & 1\end{pmatrix},$$

$$\mathrm{S}=\begin{pmatrix}\mathrm{U}_i^T & 0\\ 0 & 1\end{pmatrix}\begin{pmatrix}\mathrm{I}_2 & 0 & 0\\ 0 & -\mathrm{I}_3 & 0\\ 0 & 0 & 1\end{pmatrix}\begin{pmatrix}\mathrm{U}_i & 0\\ 0 & 1\end{pmatrix},$$

$\mathbf{d}_1 = (\mathbf{v}_i^T, 1)\mathrm{D}_{12}^T$, $d_2 = (\mathbf{v}_i^T, 1)\mathrm{D}_{22}\binom{\mathbf{v}_i}{1}$, $\mathbf{s}_1 = (\mathbf{v}_i^T, 1)\mathrm{S}_{12}^T$, $s_2 = (\mathbf{v}_i^T, 1)\mathrm{S}_{22}\binom{\mathbf{v}_i}{1}$, D_{11} and S_{11} are the upper-left $m_i \times m_i$ submatrix of D and S, D_{12} and S_{12} are the upper-right $m_i \times (6-m_i)$ submatrices of D and S, D_{22} and S_{22} are the lower-right $(6-m_i)\times(6-m_i)$ submatrices of D and S, respectively.

By Lagrange's multiplier method, we obtain the following Lagrange's equations according to (22):

$$\begin{cases}(\mathrm{D}_{11}+\gamma\mathrm{S}_{11})\boldsymbol{\mu}_i+\mathbf{d}_1+\gamma\mathbf{s}_1=0\\ \boldsymbol{\mu}_i^T\mathrm{S}_{11}\boldsymbol{\mu}_i+2\mathbf{s}_1\boldsymbol{\mu}_i+s_2=0\end{cases}\tag{23}$$

where γ is a multiplier. Here, three cases need to be considered respectively and the optimal solution is selected from the candidates of $\boldsymbol{\mu}_i$ in these three cases.

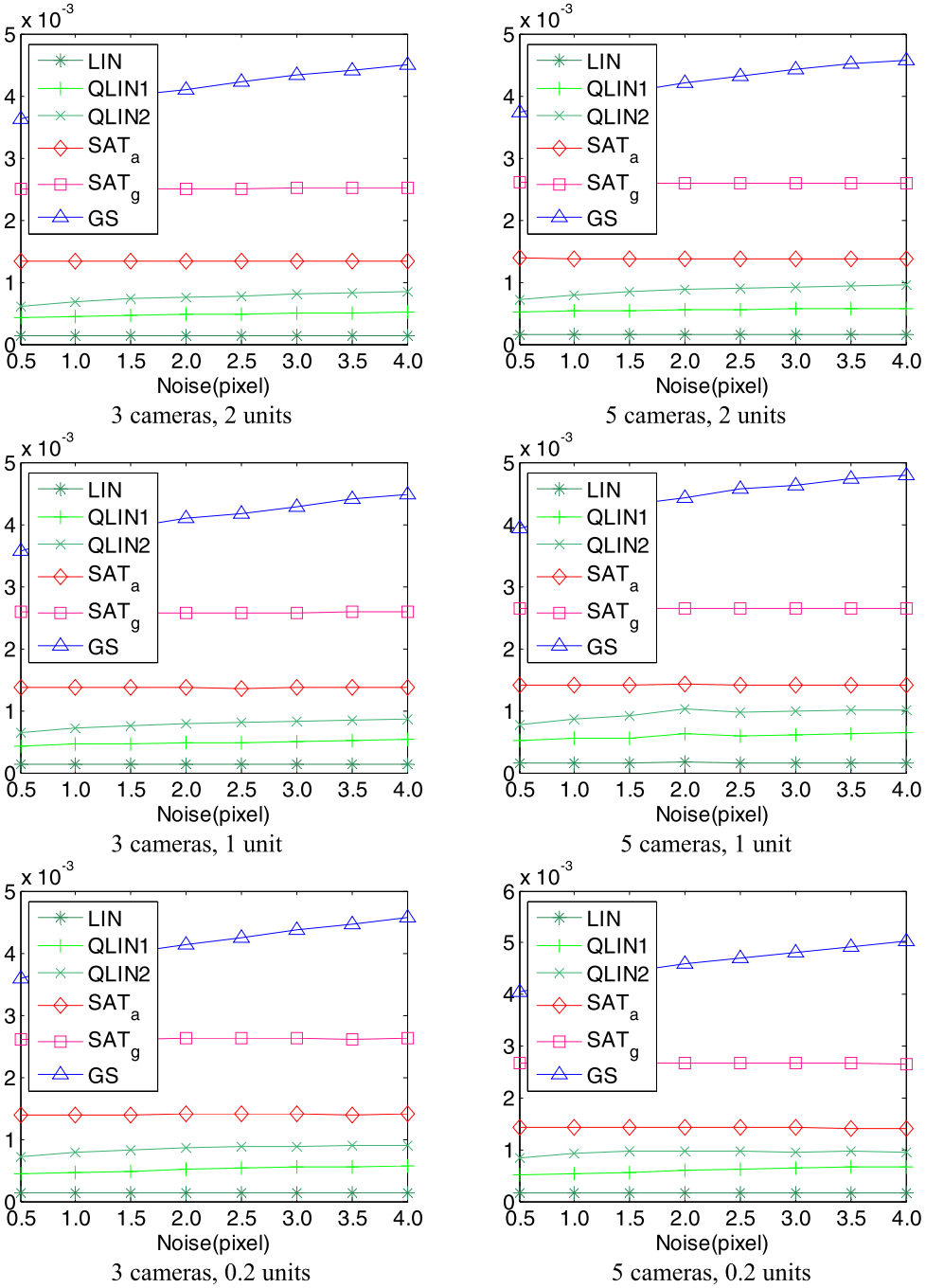

Fig. 9 Experimental results of the Configuration II. Average of running time (second)

Case A: $\det(\mathrm{D}_{11} + \gamma \mathrm{S}_{11}) \neq 0$

According to the first equation in (23), we obtain

$$\boldsymbol{\mu}_i = -\frac{(\mathrm{D}_{11} + \gamma \mathrm{S}_{11})^* (\mathbf{d}_1 + \gamma \mathbf{s}_1)}{\det(\mathrm{D}_{11} + \gamma \mathrm{S}_{11})} \tag{24}$$

where $(\mathrm{D}_{11} + \gamma \mathrm{S}_{11})^*$ is the adjoint matrix of $\mathrm{D}_{11} + \gamma \mathrm{S}_{11}$. Substituting (24) into the second equation of (23), an equation of degree $2m_i$ $(2 \leq m_i \leq 4)$ is obtained

$$\begin{aligned}&(\mathbf{d}_1 + \gamma \mathbf{s}_1)^T (\mathrm{D}_{11} + \gamma \mathrm{S}_{11})^{*T} \mathrm{S}_{11} (\mathrm{D}_{11} + \gamma \mathrm{S}_{11})^* (\mathbf{d}_1 + \gamma \mathbf{s}_1) \\ &\quad - 2 \det(\mathrm{D}_{11} + \gamma \mathrm{S}_{11}) \mathbf{s}_1 (\mathrm{D}_{11} + \gamma \mathrm{S}_{11})^* (\mathbf{d}_1 + \gamma \mathbf{s}_1) \\ &\quad + s_2 \det(\mathrm{D}_{11} + \gamma \mathrm{S}_{11})^2 = 0\end{aligned} \tag{25}$$

Because the order of the square matrix $\mathrm{D}_{11} + \gamma \mathrm{S}_{11}$ is not more than 4, its determinant and adjoint matrix can be computed easily. By choosing real roots of (25) which do not make $\det(\mathrm{D}_{11} + \gamma \mathrm{S}_{11}) = 0$ and substituting them into (24), we can obtain the candidates of $\boldsymbol{\mu}_i$.

Case B: A root γ' of $\det(D_{11} + \gamma S_{11}) = 0$ makes the first equation in (23) solvable and only one eigenvalue of matrix $D_{11} + \gamma' S_{11}$ is zero.

Referring to Situation $m_i = 1$, by the eigen-decomposition of $D_{11} + \gamma' S_{11}$, an equation like (20) is obtained. Substituting the equation into the second equation of (23), if there exists real roots, like Situation $m_i = 1$ the candidates of $\boldsymbol{\mu}_i$ can be obtained with the real roots.

Case C: A root γ'' of $\det(D_{11} + \gamma S_{11}) = 0$ makes the first equation in (23) solvable and more than one eigenvalue of the matrix $D_{11} + \gamma'' S_{11}$ are zero.

The problem returns to Situation $m_i > 1$. By the eigen-decomposition of $D_{11} + \gamma'' S_{11}$, an equation like (21) is obtained, then a minimization problem like (22) is constructed, which can be solved just like Case A, Case B and Case C. Because the Case C is similar to Situation $m_i > 1$, the details to obtain the candidates of $\boldsymbol{\mu}_i$ will be skipped here.

References

1. Hartley, R., Sturm, P.: Triangulation. Comput. Vis. Image Underst. **68**(2), 146–157 (1997)
2. Wu, F.C., Zhang, Q., Hu, Z.Y.: Efficient suboptimal solutions to the optimal triangulation. Int. J. Comput. Vis. **91**(1), 77–106 (2011)
3. Kanatani, K., Sugaya, Y., Niitsuma, H.: Triangulation from two views revisited: Hartley-Sturm vs. optimal correction. In: Proceedings of the British Machine Vision Conference, pp. 173–182 (2008)
4. Lindstrom, P.: Triangulation made easy. In: Proc. Computer Vision and Pattern Recognition, pp. 1554–1561 (2010)
5. Olsson, C., Kahl, F., Okarsson, M.: Branch and bound methods for Euclidean registration problems. IEEE Trans. Pattern Anal. Mach. Intell. **31**(5), 783–794 (2009)
6. Olsson, C., Kahl, F., Hartley, R.: Projective least-squares: global solutions with local optimization. In: Proc. Computer Vision and Pattern Recognition, pp. 1216–1223 (2009)
7. Lu, F., Hartley, R.: A fast optimal algorithm for L_2 triangulation. In: Proc. Asian Conference on Computer Vision, pp. 279–288 (2007)
8. Hartley, R., Schaffalitzky, F.: L_∞ minimization in geometric reconstruction problems. In: Proc. Computer Vision and Pattern Recognition, pp. 504–509 (2004)
9. Ke, Q., Kanade, T.: Quasiconvex optimization for robust geometric reconstruction. IEEE Trans. Pattern Anal. Mach. Intell. **29**(10), 1834–1847 (2007)
10. Kahl, F., Hartley, R.: Multiple-view geometry under the L_∞-norm. IEEE Trans. Pattern Anal. Mach. Intell. **30**(9), 1603–1617 (2008)
11. Xiao, J., Fang, T., Tan, P., Zhao, P., Ofek, E., Quan, L.: Image-based facade modeling. ACM Trans. Graph. **27**(5), 1–10 (2008)
12. Xiao, J., Fang, T., Zhao, P., Maxime, L., Quan, L.: Image-based street-side city modeling. ACM Trans. Graph. **28**(5), 1–12 (2009)
13. Agarwal, S., Snavely, N.: Building Rome in a day. In: Proc. International Conference of Computer Vision, pp. 72–79 (2009)
14. Beardsley, P.A., Zisserman, A., Murray, D.: Navigation using affine structure from motion. In: Proc. European Conference on Computer Vision, pp. 85–96 (1994)
15. Bartoli, A., Sturm, P.: Structure-from-motion using lines: representation, triangulation, and bundle adjustment. Comput. Vis. Image Underst. **100**(3), 416–441 (2005)
16. Spetsakis, M., Aloimonos, J.: Structure from motion using line correspondences. Int. J. Comput. Vis. **4**(3), 171–183 (1990)
17. Weng, J., Huang, T., Ahuja, N.: Motion and structure from line correspondences: closed-form solution, uniqueness, and optimization. IEEE Trans. Pattern Anal. Mach. Intell. **14**(3), 318–336 (1992)
18. Josephson, K., Kahl, F.: Triangulation of points, lines and conics. J. Math. Imaging Vis. **32**(2), 215–225 (2008)
19. Hartley, R., Zisserman, A.: Multiple View Geometry in Computer Vision, 2nd edn. Cambridge Univ. Press, Cambridge (2003)
20. Ressl, C.: Geometry, constraints and computation of the trifocal tensor. PhD thesis, Technical University of Vienna (2003)

Qiang Zhang received his B.S. degree from Xidian University in 2004 and received his M.S. degree in Circuits and Systems from the same university in 2007. He received his Ph.D. degree in Pattern Recognition and Intelligent System from Institute of Automation, Chinese Academy of Sciences, in 2012. He is now a lecturer in School of Electronic Engineering and a postdoctoral fellow in Key Laboratory of Intelligent Perception and Image Understanding of Ministry of Education, Xidian University. His research interests include computer vision, image processing and pattern recognition.

Yan Wu received her B.S. degree from Xidian University in 1987. She received the M.S. and Ph.D. degree in Electronic Circuit and System from the same university in 1997 and 2003, respectively. During 2003 and 2005, she was a Postdoctoral Fellow with the National Key Laboratory for Radar Signal Processing, Xidian University. She is now a Professor in School of Electronic Engineering, Xidian University. Her research interests include pattern recognition, image fusion and image processing.

Fan Wang received his B.S. degree from Xidian University in 2010. He is now a Ph.D. candidate in Electronic Circuit and System, Xidian University. His research interests include image processing, image fusion and pattern recognition.

Qiulei Dong received the B.S. degree in automation from Northeastern University in 2003, and the Ph.D. degree from the Institute of Automation, Chinese Academy of Sciences in 2008. He is currently an associate professor with the Institute of Automation, Chinese Academy of Sciences. His research interest covers pattern classification and 3D computer vision.

Licheng Jiao received the B.S. degree from Shanghai Jiaotong University in 1982 and the M.S. and Ph.D. degrees from Xi'an Jiaotong University in 1984 and 1990, respectively. During 1990 and 1991, he was a Postdoctoral Fellow with the National Key Laboratory for Radar Signal Processing, Xidian University. He is currently the Director of the Institute of Intelligent Information Processing, Xidian University. He is the author or coauthor of more than 150 scientific papers and has published 3 books. His research interests include signal and image processing, nonlinear circuit and systems theory, learning theory and algorithms, optimization problems, wavelet theory, and data mining.